

A search for L dwarf binary systems

I. Neill Reid¹, John E. Gizis², J. Davy Kirkpatrick², D. W. Koerner¹

ABSTRACT

We present analysis of HST Planetary Camera images of twenty L dwarfs identified in the course of the Two Micron All-Sky Survey. Four of the targets, 2MASSW J0746425+200032, 2MASSs J0850359+105716, 2MASSW J0920122+351742 and 2MASSW J1146345+223053, have faint, red companions at separations between 0.07 and 0.29 arcseconds (1.6 to 7.6 AU). Ground-based infrared imaging confirms the last as a common proper-motion companion. The surface density of background sources with comparable colours is extremely low, and we identify all four as physical binaries. In three cases, the bolometric magnitudes of the components differ by less than 0.3 magnitudes. Since the cooling rate for brown dwarfs is a strong function of mass, similarity in luminosities implies comparable masses. The faint component in the 2M0850 system, however, is over 1.3 magnitudes fainter than the primary in the I-band, and ~ 0.8 magnitudes fainter in M_{bol} . Indeed, 2M0850B is ~ 0.8 magnitudes fainter in I than the lowest luminosity L dwarf currently known, while the absolute magnitude we deduce at J is almost identical with M_J for Gl 229B. We discuss the implications of these results for the temperature scale in the L/T transition region. 2M0850 is known to exhibit $\lambda 6708\text{\AA}$ Li I absorption, indicating that the primary has a mass less than $0.06M_{\odot}$. Theoretical models predict that the magnitude difference implies a mass ratio of ≈ 0.75 .

The apparent binary fraction of the current sample, 20%, is comparable with the results of previous surveys of late-type M dwarfs in the field and in the Hyades cluster. However, the mean separation of the L dwarf binaries in the current sample is smaller by a factor of two than the M dwarf value, and only one system would be detected at the distance of the Hyades. We discuss the likely binary frequency amongst L dwarfs in light of these new data.

Subject headings: stars: brown dwarfs – stars: binaries

¹Department of Physics and Astronomy, University of Pennsylvania, 209 South 33rd St., Philadelphia, PA 19104-6396, inr@morales.physics.upenn.edu

²Infrared Processing and Analysis Center, MS 100-22, California Institute of Technology, Pasadena, CA 91125, davy@ipac.caltech.edu, gizis@ipac.caltech.edu

1. Introduction

The hypothesis that stars might form gravitationally-bound binary systems dates to 1783 with John Goodricke’s explanation of the periodic luminosity variations in both β Persei (Algol) and δ Cephei. Subsequent observations (reported by Pickering in 1881) confirmed at least the former case, and the frequency of binarity as a function of spectral type is now recognised as a significant constraint on global star formation theories. Moreover, binarity may influence the characteristics of planetary systems by affecting the structure and extent of protoplanetary disks.

The frequency of stellar-mass companions varies with the mass of the primary. The multiple star fraction (msf) is defined as the fraction of stellar systems which are binary or multiple. Studies of solar-type stars (Duquennoy & Mayor, 1991) indicate a high msf, exceeding 60%. In contrast, surveys of lower-mass M dwarfs find a multiplicity frequency of 35%, with companions at separations from 0.01 to 2500 AU (Fischer & Marcy, 1992; Reid & Gizis, 1997a, b). Approximately 5% of M dwarfs in the Solar Neighbourhood are companions of more massive stars (spectral type K and earlier). Overall, 60% of M dwarf systems are single.

In contrast, recent observations have resulted in the identification of a surprisingly large number of binaries amongst the lower-temperature, lower-mass L dwarfs discovered in the course of the new generation of near-infrared sky surveys. Two of the three L dwarfs in the original DENIS brown dwarf mini-survey (Delfosse *et al.*, 1997) prove to be binary (Martín *et al.*, 1999; Koerner *et al.*, 1999 - hereinafter Ko99). Three of ten L dwarfs observed by Ko99 using the Near-Infrared Camera (NIRC) on Keck are identified as binaries.

At first sight, these results suggest a high binary fraction for L dwarf systems. However, almost all of the binaries detected to date are spatially-resolved systems with equal-luminosity components at separations of < 0.5 arcseconds, unresolved in the original infrared surveys. Both the DENIS (Delfosse *et al.*, 1997) and 2MASS (Kirkpatrick *et al.*, 1999a; 2000: hereinafter K99 and K00) L dwarf samples are drawn from magnitude-limited catalogues. As pointed out by Öpik (1924) and Branch (1976), the larger effective sampling volume leads to enhanced numbers of equal-luminosity binaries under such circumstances.

We are currently undertaking a project which aims at a definitive measurement of the binary frequency amongst ultracool dwarfs (spectral types $\geq M8$) by combining high-resolution imaging with the Planetary Camera of the Hubble Space Telescope and high-resolution spectroscopy with NIRSPEC on Keck. This paper presents the first results from this programme: HST images of twenty L dwarfs, four of which are resolved as binaries. Unlike most previous discoveries, one of the systems discussed in this paper has a

secondary component significantly fainter than the system primary. That system therefore has a mass ratio, $\frac{M_2}{M_1}$ (or q), less than unity. The following section presents the observations and the final section discusses the implications of these results.

2. Observations

Table 1 lists the L dwarfs targeted for observation. All were identified based on their extremely red near-infrared colours ($(J-K_s) > 1.3$ mag.) measured in the 2MASS survey, and each has been confirmed as spectral type L based on follow-up spectroscopy. Optical spectra of 2M0850, 2M0913, 2M1146, 2M1155, 2M1328, 2M1439 and 2M1632 (we adopt this abbreviated nomenclature for each source) are presented by K99; observations of 2M0036, 2M0746 and 2M1507 are discussed by Reid *et al.* (2000); and the remaining L dwarfs are included in K00. Four of the targets have lithium absorption: 2M0825, 2M0850, 2M1146 and 2M1726 have features with equivalent widths of 10, 15, 5 and 6 Å respectively, indicating masses below $0.06 M_\odot$ (Rebolo *et al.*, 1992). The available spectroscopic observations allow us to set upper limits of 1 Å on Li 6708 Å for fourteen of the sixteen remaining dwarfs; low signal-to-noise data for 2M0708 and 2M1623 lead to upper limits of only 5 Å. All are likely to have masses close to or below the hydrogen-burning limit.

Each L dwarf was imaged on the Planetary Camera chip of WFPC2, using both F814W and F606W filters. The camera has a plate-scale of 0.0455 arcsec pix^{-1} and the F814W (I-band) exposure times were adjusted to provide the maximum dynamic range for companion detection without saturating the target. Table 2 gives the journal of observations. The analysis techniques used are discussed in Reid & Gizis (1997a, b). In brief, our observations are capable of detecting equal-luminosity binaries with separations, Δ , of more than 0.09 arcseconds, with limiting sensitivities of $\Delta I_{B-A} = 1, 3$ and 5 magnitudes at $\Delta = 0.14, 0.23$ and 0.31 arcseconds, respectively, where ΔI_{B-A} is the magnitude difference between secondary and primary. The maximum radius for companion detection, 18.2 arcseconds, is set by the angular field of view of the PC chip. The 2MASS scans allow us to search for L- and T-dwarf companions brighter than $J=16$ at wider separations. At the average distance of the present sample, 20 parsecs, equal-luminosity binaries are detectable at separations between 1.8 and 360 AU.

Accurate positions for each source (from 2MASS) are given in Table 1, where we also list spectral types, parallax estimates and both I-band and infrared photometry. The trigonometric parallax measurements are from USNO observations (Dahn et al, 1999), updated in a few cases to include more recent observations (Dahn, priv. comm.). Only nine L dwarfs, including three binaries, have ground-based I_C photometry from USNO

observations (Dahn *et al.*, 1999). However, we have used DAOPHOT to measure I_{814} magnitudes for all of the sources, adopting the zeropoint derived in Holtzman *et al.*'s (1995) calibration. Clearly, all of our targets are significantly redder than any of the calibrating stars observed by Holtzman *et al.*, and we have used the six apparently single dwarfs in this sample to determine the extent of any colour term. Figure 1 shows the results: the available data can be represented by a linear correction

$$\delta I = I_C - I_{814} = -(0.534 \pm 0.439) + (0.230 \pm 0.121)(I_{814} - J)$$

Neither the slope nor the zeropoint of the fit is strongly constrained. However, the dispersion about the relation is only 0.06 magnitudes, and eliminating the single most discrepant point (at $\delta I = 0.44$ mag) gives

$$\delta I = I_C - I_{814} = -(0.285 \pm 0.271) + (0.155 \pm 0.076)(I_{814} - J)$$

reducing δI by only 0.05 magnitudes at $(I_{814}-J) = 4$. These uncertainties are not important in the present context. The increase in δI at later spectral types probably reflects the steep spectral slope at $\lambda < 9000\text{\AA}$ due to broad K I $\lambda 7665/7699$ absorption. We have used the steeper relation to transform the WFPC2 I_{814} magnitudes to the Cousins I-band. (Hereafter, we use M_I to denote absolute magnitudes on the Cousins' system, and M_{814} for the HST system.) Figure 2 plots the location of our targets on the $(M_J, (I_C-J))$ plane.

The linear colour term we derive above is unlikely to be valid at redder colours. Gl 229B is the only T dwarf with HST photometry. Golimowski *et al.* (1998) measure $M_{814} = 20.76$, giving an $(I_{814} - J)$ colour of 5.26 magnitudes (adopting the J-band magnitude measured by Leggett *et al.*, 1999) and predicting $\delta I = 0.68$ magnitudes. Matthews *et al.* (1996) list the absolute magnitude as $M_i = 21.2$. While this measurement was made with a Gunn i filter, the magnitude is tied to the Cousins flux zeropoint, rather than to the AB magnitude system. Hence, the corresponding colour is $(I_C-J) = 5.68$, equivalent to $\delta I \sim 0.42$ magnitudes.

Sixteen of the twenty targets in the present sample show no evidence for duplicity in our observations; four dwarfs, however, have apparent companions at small angular separations (Figure 3). Ground-based near-infrared imaging had already identified 2M1146 as a likely binary source (Ko99). Our HST imaging confirms that observation, and, using DAOPHOT, we measure a separation of 0.29 arcseconds at a position angle of $199^\circ.5$, and a magnitude difference of $\Delta I_{814} = I_{814}(B) - I_{814}(A) = 0.31$ magnitudes. This compares with $\Delta = 0.29$ arcseconds, $\theta = 206^\circ$ and $\Delta K = 0.1$ magnitudes derived from NIRC observations (Ko99).

Reid *et al.* (2000) suggested 2M0746 as a binary candidate based on its location in the $(M_J, (I-J))$ colour-magnitude diagram, 0.7 magnitudes brighter than the ‘‘main sequence’’.

This suggestion proves to have merit, with the two components having $\Delta I_{814} = 0.62$ mag and a separation of 0.22 arcseconds. 2M0920 is barely resolved, but is clearly extended in the F814W image. Fitting the image profile using our 2M0036 observation as a PSF template, we derive $\Delta I_{814} = 0.4$ mag and $\Delta = 0.07$ arcseconds.

The fourth binary candidate, 2M0850, is notable in that the resolved companion, lying at a separation of 0.16 arcseconds, is significantly fainter than the primary. We measure a relative magnitude of $\Delta I_{814} = 1.27$ magnitudes. The individual magnitudes, based on Holtzman *et al.*'s (1995) calibration, are $I_{814} = 20.44$ and 21.76 magnitudes, and the fainter source is not detected in the F606W observation.

Are these apparent companions physically associated with the L dwarf targets? As Table 2 shows, all four candidate binaries lie at moderate to high Galactic latitude, with a correspondingly low surface density of background stars. There is no evidence that any of the companions is spatially extended, as might be expected for background galaxies, although limits are less stringent for 2M0920. We have used standard filtering techniques to remove cosmic rays from the images, and Table 2 lists the number of faint ($I_{814} < 20.5$), stellar sources in each Planetary Camera frame. The average surface density is 6.5 ± 3.6 sources per PC frame, implying an *a priori* probability of $\sim 3 \times 10^{-4}$ of finding a source within 0.16 arcseconds of a given point on the frame. Even in the more crowded field of 2M0920, the probability of association, given a random distribution of background sources, is only 4×10^{-3} .

Coincidence arguments are vulnerable to small number statistics. However, faint background sources are expected to be either K-type Galactic stars or low-redshift ($z < 0.5$) galaxies with similar colours, and all of the background sources we detect have neutral ($R_{606} - I_{814}$) colours. In contrast, all of the potential companions have (R-I) colours similar to the known L dwarf primaries, significantly redder than either K-type stars or galaxies. As a final test, Koerner & Kirkpatrick have deep near-infrared images ($K < 22$ mag.) of all four sources, obtained with the Keck telescope 1 to 2 years before the HST observations. 2M1146A/B is confirmed as a common proper-motion pair. The motions of 2M0746 and 2M0850 (0.38 and 0.16 arcsec yr⁻¹ respectively, Dahn *et al.*, 1999) are sufficient that the companions should be resolved if either were a stationary background source: no such object is visible in either set of NIRC images. Thus, the preponderance of the evidence indicates that all four faint sources are physical companions of the respective L dwarf targets.

3. Discussion

3.1. Absolute magnitudes and luminosities

Adopting the hypothesis that the sources are physically associated, Table 3 lists the absolute magnitudes derived for the individual components. We have used the relative fluxes measured from the WFPC2 F814W images to deconvolve the relative contribution of each star to the joint I-band photometry. We use a similar technique to estimate the individual J magnitudes. The L dwarf sequence has a slope of ~ 4 in the $(M_I, (I_C-J))$ colour-magnitude plane (Figure 4), and we estimate the relative magnitudes at $1.25\mu\text{m}$ using

$$\Delta J \approx 0.75 \times \Delta I_C$$

Absolute magnitudes for each component can then be derived from $M_J(\text{AB})$.

Figure 4 plots the location of each component in the $(M_I, (I_C-J))$ plane. The two most luminous systems, 2M0746 and 2M1146, are both overluminous in Figure 2, which plots the joint, ground-based photometry. Figure 4 shows that the individual components of both systems lie squarely within the L dwarf sequence³. These are two of the brightest L dwarfs known; indeed, 2M0746 is currently the brightest, with an apparent magnitude of $K=10.49$. The fact that both prove to be binaries, as have two of the three bright L dwarfs discovered in the initial DENIS brown dwarf minisurvey (Delfosse *et al.*, 1997), is a clear example of Öpik’s equal-mass binary selection effect.

Considering the two later-type binaries, both components in 2M0920 lie 0.3 magnitudes blueward of the L dwarf sequence. That system currently lacks a trigonometric parallax, and the absolute magnitudes are correspondingly less certain. Both components in 2M0850AB lie squarely on the sequence. There is something of a discrepancy between the observed spectral type, L6, and the absolute magnitude of 2M0850A, which is slightly fainter than the value derived for the L7.5 dwarf, 2M0825. This may simply reflect intrinsic scatter in the $(M_I, \text{spectral type})$ relation.

Given these observations, we have attempted the derivation of luminosities of these systems. In principle, theoretical models can be used for this purpose. However, the flux distribution of ultracool dwarfs is affected by atmospheric dust, which starts to form at approximately spectral type M6. The emergent energy distribution predicted by stellar models is dependent strongly on the assumption made concerning the distribution of that dust, as illustrated most dramatically by Chabrier *et al.* (2000): dust-free and dusty

³ Two unresolved systems are noticeably over luminous in Figure 4: PC0025, at $M_I = 15.5$, $(I_C-J)=3.7$; and 2M1328, at $M_I = 17.2$, $(I_C-J)=4.1$. Burgasser *et al.* (2000a) suggest that the former is an interacting red dwarf/brown dwarf binary. Both would repay further study.

models differ by over 2 magnitudes in (J- K_S); bolometric corrections have correspondingly large uncertainties. These problems are particularly acute for L-type dwarfs. Under such circumstances, we prefer to rely on empirical measurements.

Even so, it is clear that there is room for improvement in the definition of empirical bolometric corrections for late-type dwarfs. Figure 5 illustrates the current state of knowledge, plotting the available J-band and I_C bolometric corrections. While we have reliable measurements for Gl 229B (from Leggett *et al.*, 1999), the latest type L dwarf with a bolometric magnitude estimate is the L4 dwarf GD 165B (Jones *et al.*, 1994; Kirkpatrick *et al.*, 1999b). Figure 5 plots those data, together with absolute magnitudes and bolometric corrections for the L2 dwarf, Kelu 1 (Ruiz *et al.*, 1997), and the M9.5 dwarf, BRI0021-0021 (Tinney *et al.*, 1993). The arrows in the upper panel for Figure 5 mark the observed locations of 2M0850A and 2M0850B.

We estimate M_{bol} for the binary components using two techniques: first, we use linear interpolation in the (M_I , BC_I) diagram. This approach may overestimate BC_I (M_{bol} too bright) in later-type L dwarfs, since the bolometric correction must depend strongly on the extent of KI absorption, which is unlikely to increase in such a simple manner from L4 to T. Second, we combine the M_J values listed in Table 3 with an estimated $BC_J=1.9$ magnitudes (lower panel, Figure 5). Averaging those estimates, which generally agree to within 0.3 magnitudes, gives the values of $\langle M_{bol} \rangle$ listed in Table 3. Luminosities are calculated for an adopted value of $M_{bol\odot} = 4.72$.

2M0850B stands out as particularly intriguing object. The I-band absolute magnitude is ~ 0.9 magnitudes fainter than the L8 dwarf 2M1632 (Table 1), while the estimated J-band absolute magnitude, $M_J \sim 15.2$, is 0.2 magnitudes fainter than faintest L dwarf currently known, Gl 584C (K00), and only 0.3 magnitudes brighter than the value measured for Gl 229B (Leggett *et al.*, 1999). Given these absolute magnitudes, the companion could be either a late-type L dwarf, spectral type $\approx L9$, or an early-type T dwarf. We discuss this system in more detail in section 3.3.

3.2. Masses and temperatures

Our HST observations provide direct measurement of the relative magnitudes of the components; transforming those data to estimates of effective temperature and mass is not straightforward. Brown dwarfs evolve rapidly in luminosity and temperature as a function of mass. The components of a binary system, however, can be assumed to be coeval. Hence, the difference in luminosity observed for 2M0850A/B must be interpreted as a difference in

mass. This is in contrast to most other known L dwarf binaries, where both components have near-equal luminosity and hence near-equal mass. L dwarfs and T dwarfs are known as secondary components of main-sequence stars (eg Gl 229B, Nakajima *et al.*, 1995; G196-3, Rebolo *et al.*, 1998), but at much wider separations (30 to 4000 AU). 2M0850A/B provides direct evidence that unequal-mass brown dwarf binaries can form at separations of < 10 AU.

Evolutionary tracks for brown dwarfs of different masses lie in close proximity in the HR diagram, overlapping tracks for low-mass stars at higher luminosities. As a result, the mass-luminosity relation is not single-valued in this régime, and we cannot estimate reliable masses for individual objects without knowledge of their age. However, if we can determine the bolometric magnitude of each component in a brown dwarf binary, we can use models to estimate a mass ratio based on the relative luminosity.

Given the luminosity estimates in Table 3, we have used theoretical models computed by Burrows *et al.* (1993, 1997) to constrain the values of relative masses in the lower luminosity systems, 2M0920 and 2M0850. As noted above, the presence of lithium in the optical spectrum of 2M0850 sets an upper limit of $0.06 M_{\odot}$ on the mass of the primary component in that system. Both components of 2M0920AB have a luminosity similar to the value for 2M0850A, but spectroscopic observations set an upper limit of 0.5\AA for the equivalent width of the Li 6708 \AA line. Theoretical models predict that lithium is removed from the gas phase as solid LiCl at low temperatures (Fegley & Lodders, 1996; Burrows & Sharp, 1999; Lodders, 1999), and spectroscopy of L dwarfs indicates that the strength of Li 6708 \AA when detected, decreases amongst the latest spectral types (K00). However, $\sim 50\%$ of L6/L6.5 dwarfs have detectable lithium, so it is more reasonable to assume that the absence of lithium in 2M0920 is due to destruction through fusion, rather than solidification. In that case, both components in 2M0920AB have masses exceeding $0.06M_{\odot}$.

Accepting these hypotheses, Figure 6a superimposes the luminosity estimated for each of the four binary components on the $(\log(L), \log(\text{age}))$ plane. Figure 6b plots the corresponding mass ratios, q . In both cases, the latter parameter varies over a relatively small range, with $q \sim 0.96$ for 2M0920AB and $q \sim 0.75$ for 2M0850AB. This sets an upper limit of $0.05 M_{\odot}$ for the mass of 2M0850B.

The Burrows *et al.* (1993, 1997) models also allow us to estimate approximate temperatures for each component, given a particular value for the primary mass (i.e. age). Table 4 lists those values, where we have interpolated between tracks as necessary. We note that there are some inconsistencies, particularly at low masses/young ages: for example, if 2M0850A has $M \sim 0.02M_{\odot}$, Figure 6a implies $\tau \sim 0.19$ Gyrs and $\sim 0.015M_{\odot}$ for 2M0850B; a $0.015M_{\odot}$ brown dwarf is predicted to have a $\log(\frac{L}{L_{\odot}}) \sim -4.7$ at that age, however, rather

than the observed $\log(\frac{L}{L_{\odot}}) \sim -4.9$. Nonetheless, these calculations provide a preliminary indication of the properties of the components in each system.

Figure 7 illustrates the results, superimposing on the theoretical H-R diagram the error boxes for both components of 2M0850 and for 2M0920A. The similarity in spectral types between the composite spectra of the two systems suggests that 2M0850A lies near the upper limit of the estimated mass range. The most probable masses for the individual components are therefore:

$$\begin{aligned} 2M0850A: & 0.05 \pm 0.01 M_{\odot} \\ 2M0850B: & 0.04 \pm 0.01 M_{\odot} \\ 2M0920A: & 0.068 \pm 0.008 M_{\odot} \\ 2M0920B: & 0.068 \pm 0.008 M_{\odot} \end{aligned}$$

There are fewer constraints on the masses of the components in the two earlier-type binaries. As with 2M0850, lithium absorption in 2M1146 indicates masses below $0.06M_{\odot}$ for both primary and secondary. 2M0746, in contrast, is lithium free, and if the system is older than ~ 1 Gyr, the Burrows *et al.* models predict that both components exceed the hydrogen-burning mass limit; at age 10 Gyrs, both have masses of $0.085M_{\odot}$.

Reliable masses require orbit determination. Such measurements should be possible over a reasonable timescale for at least two of the four systems discussed here. The average observed separation of components in a binary system is eighty percent of the semi-major axis. Applying that rule of thumb to our observations, and taking the mass limits estimated above, 2M0850AB is likely to have an orbital period of 43 years, while 2M0920AB may have a period as short as 8.5 years. The latter system may be amenable to astrometry with the next generation of optical interferometers. 2M0746 may be accessible to more conventional imaging: with a lower mass limit of $0.12 M_{\odot}$ (total mass), a semi-major axis of 3.5 AU implies a period of less than 18 years. In contrast, 2M1146 ($M_{tot} < 0.12M_{\odot}$) with $\langle a \rangle \sim 9.5$ AU has a likely period exceeding 85 years.

3.3. Temperature scales, 2M0850 and the L/T transition

The extensive observational and theoretical work undertaken over the last few years has led to the emergence of a convincing qualitative scenario for brown dwarf spectral evolution. As the atmosphere cools below an effective temperature of $\sim 2500\text{K}$, first TiO and then VO solidify as dust particles, leaving metal hydrides as the strongest molecular features in the optical spectrum. The removal of these major opacity sources leads to increased atmospheric transparency, which in turn accounts for the presence of strong,

pressure-broadened atomic lines of alkali metals (Na, K, Cs, Rb, Li). At near-infrared wavelengths, H₂O absorption dominates the spectrum, with CO a prominent feature at 2.03 μ m. As originally predicted by Tsuji (1964), carbon is bound preferentially in methane, rather than CO, at low temperatures, leading to strong absorption in the H and K windows, as in Gl 229B. This accounts for the blue near-infrared colours of T dwarfs such as Gl 229B and Gl 570D.

The qualitative picture is clear. Quantitatively, however, we still lack a well-grounded temperature scale to associate with this behaviour. The threshold temperature (if, indeed, there is a clean threshold) for the onset of methane absorption at 2 μ m is important not only in understanding the structure of individual brown dwarfs, but also in disentangling the underlying mass function from the observed number/spectral type surface densities (Reid *et al.*, 1999). In broad terms, two temperature calibrations have been suggested. Basri *et al.* (2000) have combined model atmosphere calculations with high-resolution line profiles to derive temperatures of \sim 2200K for spectral type L0 and \sim 1700K for type L8 (K99 classification system). Noll *et al.* (2000) argue that the relatively weak 3.3 μ m fundamental-band methane absorption detected in mid- and late-type L dwarfs favours this relatively hot scale, which implies a \sim 700K temperature difference between the latest L dwarfs and Gl 229B. If this temperature scale is correct, then there is a substantial population of early-type T dwarfs in the Solar Neighbourhood, at least equal in number density to the known L dwarf population.

Photometric analyses, however, suggest lower temperatures. At least four currently-known L8 dwarfs have values of M_J within 1 magnitude of Gl 229B ($M_J = 15.5$): 2M1632, $M_J = 14.7$ (Table 1), SDSSp J132629.82-003831.5 ($M_J=14.8$; Fan *et al.*, 2000), 2MASSW J0310599+164816 ($M_J = 14.9$, K00) and 2MASSW J1523226+301456 ($M_J = 15.0$, K00). The last mentioned dwarf is particularly important, since it is a proper-motion companion of the known nearby G-dwarf binary, Gl 584AB, and therefore has a well-determined trigonometric parallax.

Late L dwarfs and T dwarfs have radically different colours: L8 dwarfs have (I-J) \approx 4.2, (J-K) \approx 2, as compared with (I-J) \approx 5.7 and (J-K) \approx 0 for Gl 229B. However, those differences are tied strongly to the relative strength of individual absorption features, broad KI at I and CH₄ overtone bands at H and K, rather than substantial variation in the underlying energy distribution. In contrast, the J-band is largely free of significant absorption features: the crucial question is how well the flux in that passband tracks bolometric magnitude. Is $\frac{F_J}{F_{bol}} \approx$ constant, as Figure 5 suggests? The scarcity of mid-infrared data for ultracool dwarfs means that we cannot answer this question directly at present; however, we can examine some of the consequent eventualities.

Gl 229B, the original T dwarf, has an effective temperature of $960 \pm 70\text{K}$ (Marley *et al.*, 1996). Since brown dwarf radii are set by degeneracy, we know that 2M1523 (Gl 584C) and Gl229B have radii which differ by at most 15%. We have

$$\frac{L_1}{L_2} = \left(\frac{R_1}{R_2}\right)^2 \left(\frac{T_1}{T_2}\right)^4$$

Suppose that Gl 584C is a high-mass brown dwarf, with a radius 15% smaller than that of Gl 229B. In that case, if Gl 584C has $T_{eff} = 1700\text{K}$, then $L_{Gl584C} \sim 5.5L_{Gl229B}$, or $M_{bol} = 15.5$, and the J-band bolometric correction is only -0.5 magnitudes. On the other hand, if we assume that the bolometric corrections outlined in Figure 5 are reliable, then $L_{Gl584C} \sim 2L_{Gl229B}$. In that case, assuming a 15% difference in radius, Gl 584C is predicted to have a temperature 30% higher than that observed for Gl 229B. That is, the photometric temperature estimate for spectral type L8 is $1250 \pm 100\text{K}$ (K00), $\sim 250\text{K}$ cooler than Basri *et al.*'s spectroscopic estimate.

Figure 2 underlines visually the photometric hypothesis, which is essentially a continuity argument. The L dwarf sequence spans a three magnitude range in the J band, $12 \leq M_J \leq 15$; Basri *et al.* assign a corresponding temperature range of 500K. Under this scenario, the 0.5 magnitude range $15 \leq M_J \leq 15.5$ between Gl 584C and Gl 229B corresponds to a temperature difference of 700K. The corresponding photometric calibration assigns a temperature difference of $\sim 750\text{K}$ (2000 to 1250K) to the L dwarf sequence, and $\sim 250\text{K}$ to the latter interval.

The discovery by the SDSS collaboration of three field brown dwarfs with both CO and CH₄ absorption (Leggett *et al.*, 2000) will clearly contribute valuable information on this problem. The co-existence of CO and methane in so many systems is surprising, since theoretical models predict their co-existence over a relatively narrow range in temperature (Fegley & Lodders, 1996). This apparent paradox might be resolved through a combination of two factors: first, binarity (as discussed further below); and, second, the non-grey nature of late-L/T-dwarf atmospheres. As with Jupiter, topographical structures (bands, spots, zones) may allow us to see to different depths at different physical locations: that is, the overall energy distribution is produced by a range of temperatures, rather than being characterised by a single effective temperature, as is usually taken to be the case in hotter stellar atmospheres. For example, the 3.3 μm methane fundamental band is believed to be produced at higher levels in the atmosphere (lower pressure, lower temperature) than are responsible for the “continuum” flux in late L dwarfs. Under such inhomogeneous conditions, both CO and the overtone 1.6 and 2.1 μm CH₄ bands might be detectable in brown dwarfs spanning a broader range in luminosity than expected.

As yet, none of the SDSS T dwarfs has a known luminosity. 2M0850AB has a measured

trigonometric parallax, allowing us to locate both components on the HR diagram (Figure 4). Thus, this system, and others like it, offer the prospect of providing valuable insight into this matter by linking the unknown (2M0850B) with the barely known (2M0850A).

The onset of detectable methane absorption in the K window defines the transition from spectral class L to class T (K99). Photometrically, however, we must make a distinction between cool dwarfs like Gl 229B, with near-saturated methane absorption in the H and K bands and A-type near-infrared colours, and the objects discovered recently by Leggett *et al.* The latter are, by definition, T dwarfs, since CH₄ is evident at K, but their near-infrared colours are closer to those of M giants, reflecting the weaker CH₄ absorption. We will refer to these objects as early-type T dwarfs, and describe the more familiar Gl 229B-like objects as ‘classical’ T dwarfs.

Given its absolute magnitude, 2M0850B might be a very late-type L dwarf, an early-type T dwarf or a ‘classical’ T dwarf. High spatial-resolution near-infrared photometry would allow us to discriminate amongst these options, since each occupies a distinct location in the (J-H)/(H-K) plane. Currently, we lack such data, but the ground-based photometry listed in Table 1, together with K-band spectroscopy (K99), allow us to set limits on the nature of the companion. Based on the slope of the (M_I , (I-J)) L dwarf sequence, we inferred $\Delta J_{B-A} \sim 1$ magnitude, which implies that 2M0850B supplies $\sim 30\%$ of the flux at $1.25\mu\text{m}$ in joint photometry. Late-type L dwarfs have similar (J-K) colours, so one would expect a similar contribution at K in an L-dwarf/L-dwarf binary system. In contrast, Gl 229B loses $\sim 70\%$ of its K-band flux to methane absorption, so, given the same ΔJ_{B-A} , an L-dwarf/classical T-dwarf system would be ~ 0.2 magnitudes bluer in (J-K) than an L-dwarf/L-dwarf binary. L-dwarf/early T-dwarf binaries will have intermediate (J-K) colours.

2M0850AB has a (J-K) colour of 1.85 ± 0.06 magnitudes. In comparison, 2M0825 and 2M1632, the two apparently-single L dwarfs closest to 2M0850A in M_I , have (J-K) colours of 1.97 ± 0.10 and 1.86 ± 0.05 magnitudes, respectively. All three dwarfs have photometry from the same source (USNO), so this comparison indicates that 2M0850 is not unusually blue for its spectral type and absolute magnitude.

We have modelled the spectrum of a hypothetical late-L/T-dwarf binary by combining our CGS4 observations of the L7 dwarf, DENIS-P 0205.4-1159 (Reid *et al.*, in prep.), with similar data for Gl 229B (Geballe *et al.*, 1996). Using IRAF, the data were binned to same scale (5\AA per pixel) and summed, adopting $\Delta J_{B-A} = 1$ magnitude. The combined spectrum is plotted in Figure 8, and compared with our K-band data for 2M0850AB (K99). The J-band magnitude difference we infer for the components corresponds to $\Delta H_{B-A} \sim 2$ magnitudes and $\Delta K_{B-A} \sim 2.6$ magnitudes. However, the extensive methane absorption

in a Gl 229B-like T dwarf leads to a significantly smaller flux difference in the shorter wavelength half of both H and K passbands, and the companion distorts the composite spectral energy distribution at those wavelengths, particularly in the H band.

Figure 8 shows that the 2M0850AB K-band observations are a reasonable match to our hypothetical composite spectrum at $\lambda > 2.15 \mu\text{m}$, but fall below the predicted flux distribution at shorter wavelengths. A T dwarf companion with strong CH_4 absorption would be expected to make the most significant contribution in the latter spectral region. Thus, the observed discrepancy argues against that option.

There is a noticeable similarity between the near-infrared spectrum of our hypothetical late-L/T-dwarf binary and data for the early-type T dwarfs identified by Leggett *et al.* (2000). Indeed, following Öpik’s binary-selection criterion, one might expect the brighter ‘early T-dwarfs’ to include a number of unresolved near equal-mass L/T binaries, with relatively small magnitude differences ΔJ_{B-A} and Δz_{B-A} . Distinguishing those objects from isolated early T dwarfs should be possible by examining the strength of the weaker methane absorption bands (for example, the $2\nu_2$ $1.67 \mu\text{m}$ feature) in both H and K bands. Broadband colours may also provide discrimination: combining a late-type L dwarf, $(J-K) \sim 1.9$, with a T dwarf companion, $\Delta J_{B-A} = 0.0$, $\Delta K_{B-A} = 1.9$, will produce a joint colour of $(J-K) \sim 1.3$ magnitudes. Bluer colours, such as those observed for three of the SDSS early-type T dwarfs, can only be produced if the companion T dwarf is *brighter* than the late-type L dwarf in the J passband. Given the relatively low opacities in the J passband and the extremely non-grey flux distribution at these low temperatures, such circumstances cannot be excluded.

Summarising the discussion, both broadband photometry and the observed K-band spectrum suggest that 2M0850B is unlikely to be a ‘classical’ T dwarf, with full blown CH_4 absorption. It remains possible that the companion is an early-type T-dwarf. Near-infrared photometry or spectroscopy of the individual components (or perhaps joint spectroscopy at H) should provide a definitive answer to this issue.

4. L dwarfs in binary systems

The ultimate goal of our program is a determination of the frequency of binary and multiple L dwarf systems. With observations of only twenty targets, our current conclusions must be tentative. Moreover, the present observing list is far from the complete, volume-limited sample which is ideally suited to this type of investigation. However, our observations are not limited to the brightest known L dwarfs, and are therefore less subject

to Öpik’s equal-mass binary selection effect. Bearing these caveats in mind, our initial results suggest that the frequency of wide binaries amongst L dwarfs is *lower* than that observed for M dwarf stars.

4.1. The HST sample

Figure 9 compares the observed magnitude difference, ΔI_{814} , for the four binaries detected in this sample against the formal detection limits for HST Planetary Camera observations (Reid & Gizis, 1997b). Those limits may be overly pessimistic: 2M0920 lies slightly below those formal limits, while 2M0850AB is easily detected, despite its proximity to the detection limit at that separation. At larger separations, the 2MASS data allow us to exclude any L dwarf companions with $J < 16$ (typically $M_J < 14.5$, $M_I < 18$) and $\Delta < 10$ arcminutes. It is clear that the detected systems occupy only a small fraction of the total parameter space available for the detection of potential companions.

The frequency of resolved binary L dwarfs in the present sample is $20 \pm 11\%$. We can match this statistic against results from three other high-resolution imaging surveys: Reid & Gizis (1997b) obtained WFPC2 images of 53 late-type M dwarfs in the Hyades cluster, identifying nine ($17 \pm 7\%$) confirmed binaries; similarly, WFPC2 observations of 41 field M dwarfs resolve 8 ($19.5 \pm 7.5\%$) as binary or multiple systems (Reid & Gizis, 1997a); finally, none of the 27 Pleiades very low-mass (VLM) dwarfs surveyed by Martín *et al.* (2000) with the NICMOS 1 camera have resolved companions. The last sample includes targets with masses comparable with those expected for our field L dwarfs, while the Hyades and field M dwarfs have higher masses, with approximate limits of $0.1 < \frac{M}{M_\odot} < 0.3$ and $0.2 < \frac{M}{M_\odot} < 0.5$, respectively.

Each of these four samples has a different mean distance. We take this into account by transforming the results to the linear régime. Taking the sensitivity limits plotted in Figure 9 as a template, we calculate the limiting absolute magnitude for companion detection as a function of separation, Δ , in AU; combining the results for each target allows us to estimate completeness limits for each sample, that is, the fraction of targets where we would expect to detect a companion with a given absolute magnitude at a given linear separation. Figure 10 plots those results, where we show the 50% and 100% detection limits together with the detected companions and the approximate absolute magnitude range of the targets.

Simple visual comparison of the four panels in Figure 10 suggests a significant difference in the semi-major axis distribution of the M dwarf and L dwarf binaries: the L dwarf binaries all have separations of less than 10 AU, while the overwhelming majority of the M

dwarf companions have $\Delta > 10$ AU. Indeed, were the L dwarfs to lie at the distance of the Hyades, we could expect to resolve only one system, 2M1146, while none would be resolved at the distance of the Pleiades. Martín *et al.* identify six Pleiades dwarfs (including PPl 15) as candidate photometric binaries. That fraction, $22 \pm 9\%$, is consistent with the statistics of our L dwarf sample, where we resolve four systems and identify 2M1328 as a candidate photometric binary.

Conversely, the wider binaries present in the M dwarf samples are not present either in our L dwarf sample or, as already noted by Martín *et al.* (2000), amongst the Pleiades VLM dwarfs. Fourteen percent of the Hyades and field M dwarfs have companions at separations between 10 and 100 AU, with a further 5% having companions in the range $100 < \Delta < 1000$ AU. A similar distribution pertains for stars in the immediate Solar Neighbourhood, with binary fractions of 5% at $\Delta \leq 1$ AU; 18% at $1 < \Delta \leq 10$ AU (compatible with our L dwarf sample); 11% at $10 < \Delta \leq 100$ AU; and 6% at $100 < \Delta \leq 1000$ AU (Reid & Gizis, 1997a). Combining our HST observations with the 2MASS limits, we would expect 3 to 4 wide ($\Delta > 10$ AU) binaries in the current sample: Martín *et al.* identified similar expectations in their analysis of the Pleiades sample. The absence of such binaries from both samples implies a 3σ deficit of wide L-dwarf binaries.

4.2. The semi-major axis distribution of brown dwarf binaries

Our HST observations are aimed at identifying low-mass binary systems. However, both L dwarfs and T dwarfs are found as companions to higher-mass main sequence stars. We have therefore made a preliminary effort to set the current results in a broader context.

Table 5 collects the available data for binary and multiple systems which include one or more ultracool dwarf component(s). With the exception of HD 10697B and the Pleiades brown dwarf, PPl 15AB, mass estimates are based on either the detection/non-detection of lithium or the estimated age of the system (usually based on the level of chromospheric activity exhibited by the main-sequence primary star). At present, the selection effects which underlie this sample are too diverse to allow detailed statistical analysis. However, two qualitative comments can be made:

- Radial velocity surveys, which have identified more than forty planetary-mass companions of nearby G dwarfs, have discovered a bare handful of brown dwarf companions with orbital semi-major axes $a < 10$ AU. This is the ‘brown dwarf desert’, highlighted by Marcy & Butler (1998). Table 5 shows that brown dwarfs exist as wide (10 to 4000 AU) companions of nearby solar-type stars. Systems with comparable

separations, but with an M dwarf as the wide component, are also known, notably Proxima Cen/ α Cen (Matthews & Gilmore, 1993).

- In contrast, all L-dwarf/L-dwarf binaries detected to date have separations of less than 10 AU, overlapping with the ‘brown dwarf desert’ in higher-mass systems, and most have mass ratios near unity. Close brown dwarfs clearly form with greater ease around low-mass primaries (cf. Basri & Martín, 1999)

Figure 11 presents these results in graphical form. The upper panel compares the (q, Δ) distribution of the the L dwarf binaries listed in Table 5 against similar data for M dwarf binaries within 8 parsecs of the Sun (from Reid & Gizis, 1997a) and for the HST M dwarf samples discussed in the previous section. Several features of this diagram demand comment:

First, there is an apparent preference for equal-mass L-dwarf/L-dwarf binaries. It remains possible that the observed distribution is partly a result of selection effects, since current observations have only limited sensitivity to low- q systems at small Δ (see Figure 10). Nonetheless, this echos the bias toward equal-mass systems amongst M dwarf binaries (Reid & Gizis, 1997a, 1997b), where observations extend to lower mass ratios.

Second, no L-dwarf/L-dwarf binaries are known with separations $\Delta > 10\text{AU}$ - is this nature or nurture? There are several possibilities: wide low-mass binaries form, but are stripped by gravitational interactions; wide binaries are inhibited from forming, leading to a truncated semi-major axis distribution and overall decrease in binary frequency; or formation of wide binaries is inhibited, but close systems form with greater frequency amongst VLM dwarfs. The last option was suggested by Basri & Martín (1999), prompted by the existence of the short-period Pleiades binary, PPl 15. Better statistics on the frequency of such binaries amongst VLM dwarfs can constrain the latter two options. We note that Mayor (2000) finds that the fraction of spectroscopic (small separation) binaries is essentially constant at $\sim 12\%$ for nearby stars with spectral types between G and M.

The third outstanding feature of the $(q, \log(\delta))$ diagram is the prevalence of low- q systems at wide separations. These are low-mass analogues of the wide, common proper motion (cpm) systems made familiar by Luyten’s extensive surveys. Such systems are vulnerable to disruption through gravitational encounters with stars and giant molecular clouds (GMCs), or via tidal effects due to the Galactic field. The binding energy of a binary star system is directly proportional to the total mass and inversely proportional to the separation. If we make the reasonable assumption that all binaries are subject to gravitational perturbations of the same average force, then we would expect to find fewer wide binaries with decreasing total system mass. Consequently, low-mass stars and brown

dwarfs in wide binaries are more likely to survive if the primary has a relatively high mass, leading naturally to a predominance of low- q systems at large Δ . Indeed, we might expect a characteristic cutoff radius for binary separation as a function of total mass, M_{tot} .

The lower panel in Figure 11 suggests strongly that there is a correlation between maximum separation and M_{tot} . Such behaviour would provide a natural explanation for the decreased *total* binary frequency amongst M dwarfs (as compared with G dwarfs), while preserving the invariance with mass of the frequency of spectroscopic binaries. However, it is not clear whether this follows the functional form expected for tidal disruption. The dotted line plotted in Figure 11 is

$$\log(\Delta_{max}) = 3.33M_{tot} + 1.1$$

i.e. a log-normal relation (the three M-dwarf binaries beyond the line are Gl 412AB, RHy 240AB and MT 3AB). One expects a scaling linearly proportional to M_{tot} for disruption by point source encounters, although circumstances are more complex in the case of an extended potential (Weinberg *et al.*, 1987). It seems unlikely, however, that the observed rapid decrease in Δ_{max} with M_{tot} is due solely to dynamical evolution.

As a final comment, we note that the wide cpm systems plotted in Figure 11 have dimensions which exceed those of typical protostellar disks. Previous studies have suggested that the relative properties of short and long-period stellar binaries may differ significantly (Mazeh *et al.*, 1992), perhaps reflecting different formation histories (Mathieu, 1994). Individual components in these wide systems may have formed essentially independently. Indeed, the widest systems may be more akin to residual cluster fragments - that is, progeny of separate cloud cores which retain the motion of the parent cluster. Under this scenario, Gl 584ABC, α Cen/Proxima, Gl 752A/VB10 and their ilk would be minimal examples of Eggen-style moving groups - cousins, rather than siblings.

Further examples of wide L-dwarf common proper motion systems will be forthcoming from detailed examination of the photometric catalogues produced by 2MASS, SDSS and DENIS. The completion of our present survey will provide more detailed information on the prevalence of ultracool dwarf binaries at modest separations.

5. Summary

We have presented high spatial-resolution Planetary Camera observations of twenty L dwarfs. Four are resolved as binary systems, with fainter companions at projected separations of 2 to 8 AU. While our present sample consists of only 20 L dwarfs, drawn from a magnitude-limited, rather than volume-limited, parent sample, the preliminary

indications are that the fraction of binary L dwarfs at separations exceeding 10 AU is lower than the empirical value of $\sim 20\%$ measured for M dwarf systems. Both L and T dwarfs, however, are found as wide companions of higher-mass, main-sequence stars.

Three of the four binaries in our current L dwarf sample here have components with similar luminosities, implying nearly equal masses; 2M0850AB, however, has a secondary component which is 1.3 magnitudes fainter than the primary. The primary has strong lithium absorption, indicating a mass below $0.06 M_{\odot}$, and comparison with theoretical models calculated by Burrows *et al.* (1993, 1997) suggests a secondary/primary mass ratio of ~ 0.8 . 2M0850B has $M_I = 19.8 \pm 0.25$, and is likely to be either a very late-type L dwarf ($\sim L9$) or an early-type T dwarf.

Unequal-mass brown dwarf binaries offer an effective means of constraining theoretical models. Since the components are coeval, both must lie on the same isochrone in the $(\log(L), \log(T_{eff}))$ plane. This technique has been used to test models of pre-main sequence stars and brown dwarfs against observations of young, multiple systems (see, for example, White *et al.*'s (1999) analysis of data for GG Tau). Once accurate effective temperatures are available for L dwarf systems, similar methods can be used to probe parameter space at lower masses and temperatures, as illustrated in Figure 7. In particular, this approach offers excellent promise for resolving questions concerning the L/T transition phase: determining both the critical threshold temperature for the onset of the change from CO-dominated spectra (L dwarfs) to CH₄ spectra (T dwarfs), and the rapidity of the transformation. More detailed observations of these, and other, binary L-dwarf systems will provide benchmarks for future theoretical models of low-mass stars and brown dwarfs.

The authors would like to thank the referee, Gibor Basri, for useful criticism. This work is based on observations with the NASA/ESA Hubble Space Telescope, obtained at the Space Telescope Science Institute, which is operated by the Association of Universities for Research in Astronomy, Inc. under NASA contract No. NAS5-26555. Our research was supported by NASA through ST ScI Grant GO-08146.01-97A.

REFERENCES

- Basri, G., Martín, E.L. 1999, AJ, 118, 2460
- Basri, G., Mohanty, S., Allard, F., Hauschildt, P.H., Delfosse, X., Martín, E.L., Forveille, T., Goldman, B. 2000, ApJ, in press
- Becklin, E.E., Zuckerman, B. 1988, Nature, 336, 656

- Branch, D. 1976, *ApJ*, 210, 392
- Burgasser, A.J., Kirkpatrick, J.D., Reid, I.N., Liebert, J., Gizis, J.E., Brown, M.E., 2000a, *AJ*, 120, 473
- Burgasser, A.B., Kirkpatrick, J.D., Cutri, R.M., *et al.* 2000b, *ApJL*, 533, L155
- Burrows, A., Hubbard, W.B., Saumon, D., Lunine, J.I. 1993, *Apj*, 406, 158
- Burrows, A., Marley, M., Hubbard, W.B., Lunine, J.I., Guillot, T., Saumon, D., Freedman, R., Sudarsky, D., Sharp, C. 1997, *ApJ*, 491, 856
- Burrows, A, Sharp, C.M. 1999, *Apj*, 512, 843
- Chabrier, G., Baraffe, I., Allard, F., Hauschildt, P. 2000, *ApJ*, in press
- Dahn, C.C., Guetter, H., Harris, H., Henden, A., Luginbuhl, C. Monet, A., Monet, D., Pier, J., Stone, R., vrba, F., Walker, R., 1999, in *From Giant Planets to Cool Stars*, (ed. C. Griffiths & M. Marley), ASP Conf. Proc. vol. 213, p. xxx
- Delfosse, X., Tinney, C.G., Forveille, T., Epchtein, N., *et al.* 1997, *Astr. Astrophys.*, 327, L25
- Duquennoy, A., Mayor, M. 1991, *Astr. Astrophys.*, 248, 485
- Fan, X., Knapp, G.R., Strauss, M.A., Gunn, J.E. *et al.* 2000, *AJ*, 119, 928
- Fegley, B., Lodders, K. 1996, *Apj*, 472, L37
- Fischer, D.A., Marcy, G.W. 1992 *ApJ*, 396, 178
- Geballe, T., Kulkarni, S.R., Woodward, C.E., Sloan, G.C. 1996, *ApJ*, 467, L101
- Gizis, J.E., Kirkpatrick, J.D., Wilson, J.C. 2000, *AJ*, submitted
- Goldman, B., Delfosse, X., Forveille, T., Afonso, C. *et al.* 1999, *Astr. Astrophys.*, 351, L5
- Golimowski, D.A., Burrows, C.J., Kulkarni, S.R., Oppenheimer, B.R., Brukardt, R.A., 1998, *AJ*, 115, 2579
- Holtzman, J.A., Burrows, C.J., Casertano, S., Hester, J.J., Trauger, J.T., Watson, A.M., Worthey, G. 1995, *PASP*, 107, 1065
- Jones, H. R. A., Longmore, A. J., Jameson, R. F., Mountain, C. M. 1994, *MNRAS*, 267, 413
- Kirkpatrick, J.D., Reid, I.N., Liebert, J., Cutri, R.M., Nelson, B., Beichman, C.A., Dahn, C.C., Monet, D.G., Skrutskie, M.F., Gizis, J. 1999a, *ApJ*, 519, 802 (K99)
- Kirkpatrick, J.D., Allard, F., Bida, T., Zuckerman, B., Becklin, E.E., Chabrier, G., Baraffe, I. 1999b, *ApJ*, 519, 834

- Kirkpatrick, J.D., Reid, I.N., Liebert, J., Gizis, J.E., Burgasser, A.J., Monet, D.G., Dahn, C.C., Nelson, B., Williams, R.J. 2000, *AJ*, 120, 447 (K00)
- Koerner, D., Kirkpatrick, J.D., McElwain, M.W., Bonaventura, N.R. 1999, *ApJL*, 526, L25
- Leggett, S.K., Toomey, D. W., Geballe, T. R., Brown, R. H. 1999, *ApJ*, 517, L139
- Leggett, S.K., Geballe, T. R. Fan, X., Schneider, D. P., Gunn, J. E., *et al.*, 2000, *ApJ*, 536, L35
- Lodders, K. 1999, *ApJ*, 519, 793
- Lowrance, P.J., McCarthy, C., Becklin, E.E., Zuckerman, B. *et al.*, 1999, *ApJL*, 512, L69
- Lowrance, P.J., Schneider, G., Kirkpatrick, J.D., Becklin, E.E. *et al.*, 2000, *ApJL*, in press
- Marcy, G.W., Butler, P. 1998, *ARAA*, 36, 57
- Marley, M.S., Saumon, D., Guillot, T., Freedman, R.S., Hubbard, W.B., Burrows, A., Luminine, J.I. 1996, *Science*, 272, 1919
- Martín, E.L., Brandner, W., Basri, G. 1999, *Science*, 283, 1718
- Martín, E.L., Brandner, W., Bouvier, J., Luhman, K.L., Stauffer, J., Basri, G., Zapatero Osorio, M.R. 2000, *ApJ*, in press
- Mathieu, R.D. 1994, *ARAA*, 32, 465
- Matthews, K., Nakajima, T., Kulkarni, S.R., Oppenheimer, B.R., 1996, *AJ*, 112, 1678
- Matthews, R., Gilmore, G. 1993, *MNRAS*, 261, L5
- Mayor, M., 2000, in *Microlensing 2000*, ed. J.W. Menzies, and P.D. Sackett, A.S.P. Conf. Proc., in press
- Mazeh, T., Goldberg, D., Duquennoy, A., Mayor, M. 1992, *ApJ*, 401, 265
- Nakajima, T., Oppenheimer, B.R., Kulkarni, S.R., Golimowski, D.A., Matthews, K., Durrance, S.T. 1995, *Nature*, 378, 463
- Noll, K.S., Geballe, T.R., Leggett, S.K., Marley, M.S. 2000, *ApJL*, in press
- Öpik, E. 1924, *Publ. Obs. Astron. Univ. Tartu*, 25, 6
- Rebolo, R., Martín, E.L., Magazzu, A. 1992, *ApJ*, 389, L83
- Rebolo, R., Zapatero Osorio, M.R., Madrugá, S., Bejar, V.J.S., Arribas, S., Licandro, J., 1998, *Science*, 282, 1309
- Reid, I.N., Gizis, J.E., 1997a, *AJ*, 113, 2246
- Reid, I.N., Gizis, J.E., 1997b, *AJ*, 114, 1992
- Reid, I.N., Kirkpatrick, J.D., Liebert, J., Burrows, A. *et al.* 1999, *ApJ*, 521, 613

- Reid, I.N., Kirkpatrick, J.D., Williams, R., Liebert, J., Burgasser, A. 2000, *AJ*, 119, 369
- Ruiz, M.T., Leggett, S.K., Allard, F. 1997, *ApJ*, 491, L107
- Shay, Z., Mazeh, T. 2000, *ApJL*, 531, L67
- Tinney, C.G., Reid, I.N., Mould, J.R. 1993, *AJ*, 105, 1045
- Tsuji, T. 1964, *Ann. Tokyo Obs. ser. II*, 9, 1
- Weinberg, M.D., Shapiro, S.L., Wasserman, I. 1987, *ApJ*, 312, 367
- White, R.J., Ghez, A.M., Reid, I.N., Schultz, G. 1999, *ApJ*, 520, 811

Table 1: Astrometric and photometric data

2MASS	Sp.	Ref.	π (mas)	M_I	(I-J)	M_J	(J-K)
WJ0036159+182110	L3.5	R00	112.4 ± 2.0^1	16.36 ± 0.05^3	3.67	12.69^3	1.38 ± 0.03
WJ0708213+295035	L5	K00	23 ± 3.5^2	17.51 ± 0.35^4	3.98	13.53	2.06 ± 0.15
WJ0740096+321203	L4.5	K00	27 ± 4^2	17.07 ± 0.35^4	3.74	13.33	1.99 ± 0.11
WJ0746425+200032	L0.5	R00	83 ± 2^1	14.69 ± 0.06^3	3.38	11.31^3	1.24 ± 0.04
WJ0820299+450031	L5	K00	28 ± 4^2	17.65 ± 0.35^4	4.13	13.52	2.06 ± 0.14
WJ0825196+211552	L7.5	K00	80 ± 12^1	18.29 ± 0.30^5	4.23	14.06^3	1.97 ± 0.10
sJ0850359+105716	L6	K99	36.1 ± 4.4^1	18.21 ± 0.25^3	4.31	13.90^3	1.85 ± 0.06
WJ0913032+184150	L3	K99	29 ± 4^2	16.83 ± 0.35^4	3.63	13.20	1.72 ± 0.09
WJ0920122+351742	L6.5	K00	48 ± 7^2	17.68 ± 0.35^4	3.73	13.95	1.66 ± 0.11
WJ0928397-160312	L2	K00	26 ± 4^2	15.96 ± 0.35^4	3.55	12.41	1.70 ± 0.07
WJ1123556+412228	L2.5	K00	20 ± 3.5^2	16.32 ± 0.35^4	3.75	12.57	1.70 ± 0.07
WJ1146345+223053	L3	K99	38.2 ± 1.3^1	15.76 ± 0.05^3	3.73	12.03^3	1.53 ± 0.04
WJ1155009+230706	L4	K99	30 ± 4.5^2	17.12 ± 0.35^4	3.73	13.39	1.68 ± 0.15
WJ1328550+211449	L5	K99	26.3 ± 4.9^1	17.19 ± 0.35^3	4.12	13.07^3	1.85 ± 0.05
WJ1338261+414034	L2.5	K00	44 ± 7^2	15.89 ± 0.35^4	3.45	12.44	1.47 ± 0.05
WJ1343167+394508	L5	K00	29 ± 4^2	17.47 ± 0.35^4	3.98	13.49	2.07 ± 0.10
WJ1439284+192915	L1	K99	69.8 ± 0.6^1	15.34 ± 0.18^3	3.43	11.91^3	1.20 ± 0.03
WJ1507476-162738	L5	R00	131.0 ± 23.2^1	17.24 ± 0.35^3	3.83	13.41^3	1.42 ± 0.03
WJ1632291+190441	L8	K99	59.5 ± 2.9^1	18.86 ± 0.11^3	4.18	14.68^3	1.86 ± 0.05
WJ1726000+153819	L2	K00	50 ± 7.5^2	18.05 ± 0.35^4	3.91	14.14^4	2.01 ± 0.08

References: K99 - Kirkpatrick *et al.*, 1999a;

K00 - Kirkpatrick *et al.*, 2000; R00 - Reid *et al.* (2000).

Notes: ¹ USNO trigonometric parallax (Dahn *et al.*, 1999);

² Photometric parallax estimate (K99/K00);

³ I_C , J and K photometry from USNO observations (Dahn *et al.*, 1999);

⁴ I_C computed from I_{814} using the relation given in section 2;

⁵ I_C from Dahn, priv. comm.

Table 2: Journal of observations

Source	Epoch	F606W Exposure	F814W Exposure	l	b	N_b^1
2M0036	15/02/2000	100s	$3 \times 100s$	119	-44 ^o	2
2M0708	23/03/2000	100s	300s, 350s	188	17	10
2M0740	27/03/2000	110s	300s, 350s	188	25	14
2M0746	15/04/2000	50s	$3 \times 50s$	201	21	5
2M0820	24/04/2000	100s	300s, 350s	175	35	7
2M0825	25/03/2000	100s	300s, 350s	203	30	10
2M0850	1/02/2000	100s	300s, 350s	209	32	3
2M0913	5/04/2000	100s	300s, 350s	211	40	5
2M0920	9/02/2000	100s	300s, 350s	189	45	16
2M0928	28/04/2000	100s	300s, 350s	249	25	3
2M1123	19/04/2000	100s	300s, 350s	169	68	5
2M1146	28/04/2000	100s	300s, 350s	228	75	6
2M1155	18/03/2000	100s	300s, 350s	229	77	8
2M1328	23/04/2000	100s	300s, 350s	0	79	4
2M1338	25/04/2000	100s	300s, 350s	91	73	3
2M1343	21/04/2000	100s	300s, 350s	84	73	5
2M1439	22/03/2000	100s	$3 \times 100s$	21	63	5
2M1507	24/02/2000	100s	$3 \times 140s$	89	34	7
2M1632	20/04/2000	100s	300s, 350s	36	39	6
2M1726	24/03/2000	100s	300s, 350s	28	25	14

¹ N_b is the number of stellar sources in each PC frame with $I_{814} > 20.5$ mag

Table 3: Binary parameters

Source	Δ	PA (deg.)	M_I	BC_I	M_{bol}	M_J	M_{bol}	$\langle M_{bol} \rangle$	$\log(\frac{L}{L_{\odot}})$
2M0746									
AB	0".22	15	14.67			11.31			
A	2.7 AU		15.17	1.5	13.7	11.85	13.75	13.75	-3.6±0.1
B			15.79	1.8	14.0	12.32	14.2	14.1	-3.75±0.1
2M0850									
AB	0".16	250	18.21			13.90			
A	4.4 AU		18.50	2.4	16.1	14.3	16.2	16.15	-4.6±0.1
B			19.84	3.0	16.8	15.2	17.1	16.95	-4.9 ± 0.1
2M0920									
AB	0".07	90	17.68			13.95			
A	1.6 AU		18.26	2.3	15.95	14.55	16.45	16.2	-4.6±0.1
B			18.70	2.6	16.1	14.9	16.8	16.35	-4.65±0.1
2M1146									
AB	0".29	199	15.76			12.03			
A	7.6 AU		16.37	1.8	14.6	12.67	14.6	14.6	-3.95±0.1
B			16.68	2.0	14.7	12.90	14.8	14.75	-4.0±0.1

Table 4: Mass estimates

2M0850				
Age (Gyrs)	$M_A(M_\odot)$	$M_B(M_\odot)$	$T_{eff}(A)$	$T_{eff}(B)$
0.19	0.02	0.015	1210	1140
0.40	0.03	0.022	1260	1100
0.71	0.04	0.031	1310	1140
1.17	0.05	0.04	1350	1160
1.72	0.06	0.047	1380	1230

Table 5: Known L dwarf/brown dwarf binaries

System	$M_{pri} (M_{\odot})$	$M_{sec} (M_{\odot})$	q^1	Δ AU	reference
PPl 15 ²	0.07	0.06	0.86	0.03	Basri & Martín, 1999
HD 10697	1.10	0.04	0.035	0.07	Shay & Mazeh, 2000
2M0746	>0.06	> 0.06	1.0	2.7	this paper
2M0920	0.06-0.075	0.06-0.075	0.95	3.2	this paper
2M0850	< 0.06	< 0.06	0.75	4.4	this paper
DENIS 1228	< 0.06	< 0.06	~ 1	4.9	Martín <i>et al.</i> , 1999
2M1146	< 0.06	< 0.06	~ 1	7.6	Ko99
DENIS 0205	0.06-0.09	0.06-0.09	~ 1	9.2	Ko99
Gl 229B	0.5	~ 0.045	~ 0.1	44	Nakajima <i>et al.</i> , 1995
TWA 5 ^{2,3}	0.4	0.025	0.06	100	Lowrance <i>et al.</i> , 1999
GD 165B	> 1	< 0.08	< .08	110	Becklin & Zuckerman, 1988
HR 7329B	~ 5	< 0.05	< .01	200	Lowrance <i>et al.</i> , 2000
GJ 1048B	~ 0.7	< 0.08	< 0.11	250	Gizis <i>et al.</i> , 2000
G196-3B	0.5	~ 0.025	~ 0.05	340	Rebolo <i>et al.</i> , 1998
GJ 1001B	0.4	~ 0.05	~ 0.13	180	Goldman <i>et al.</i> , 1999
Gl 570D	0.7	~ 0.05	~ 0.07	1525	Burgasser <i>et al.</i> , 2000b
Gl 417B	1.0	~ 0.035	~ 0.035	2000	Kirkpatrick <i>et al.</i> , in prep.
Gl 584C	1.0	~ 0.060	~ 0.060	3600	Kirkpatrick <i>et al.</i> , in prep.

¹ Mass ratios for L dwarf/L dwarf systems are based on the relative K-band luminosity

² Members of Pleiades cluster or TW Hydrae association

³ High resolution spectroscopy indicates that several other stars in this moving group are binary or multiple systems.

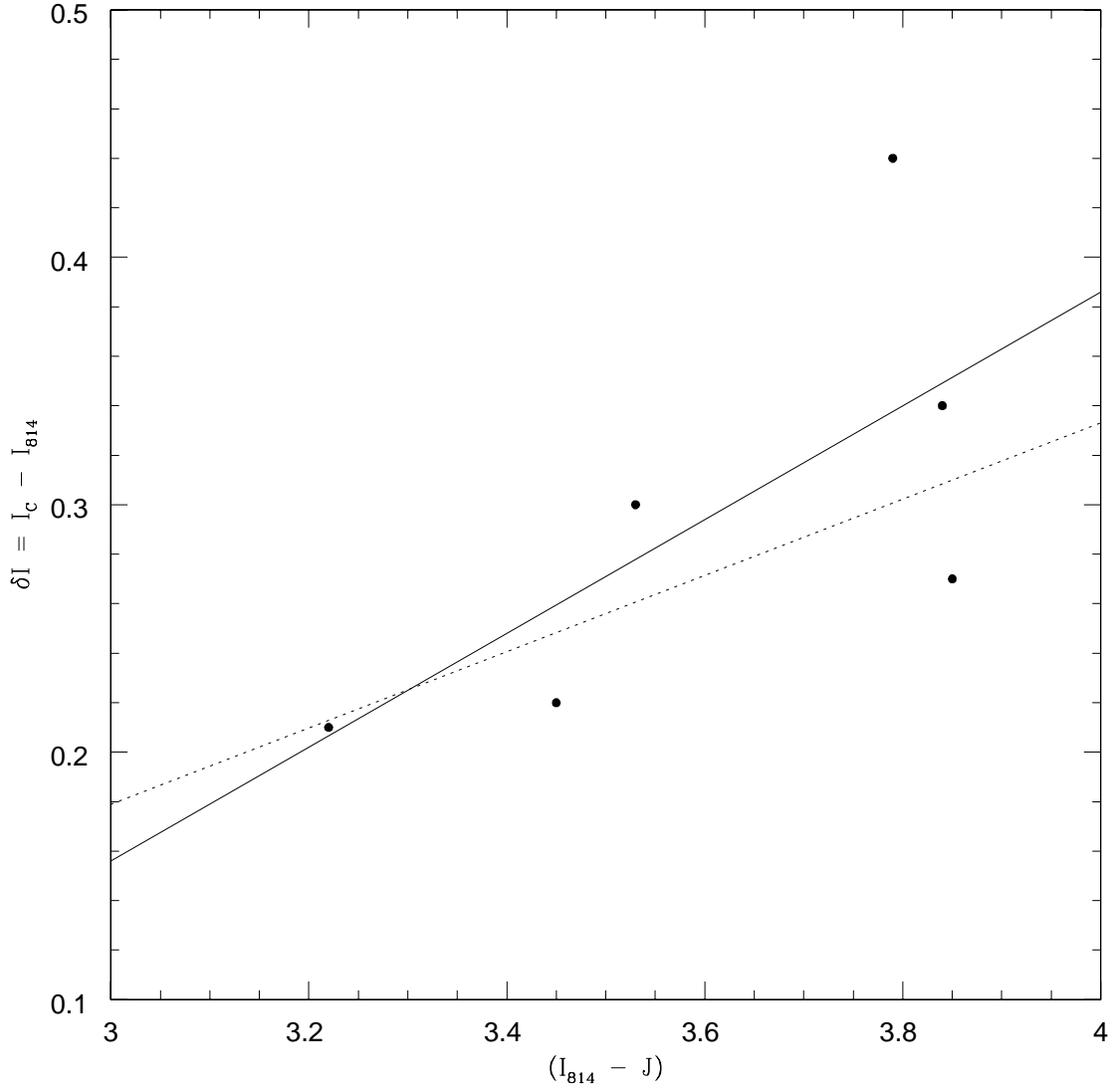


Fig. 1.— The offset between I_C and I_{814} as a function of $(I_{814}-J)$ colour for L dwarfs. The solid line plots the best-fit linear relation, the dashed line plots the linear regression if the most discrepant point is omitted from the sample..

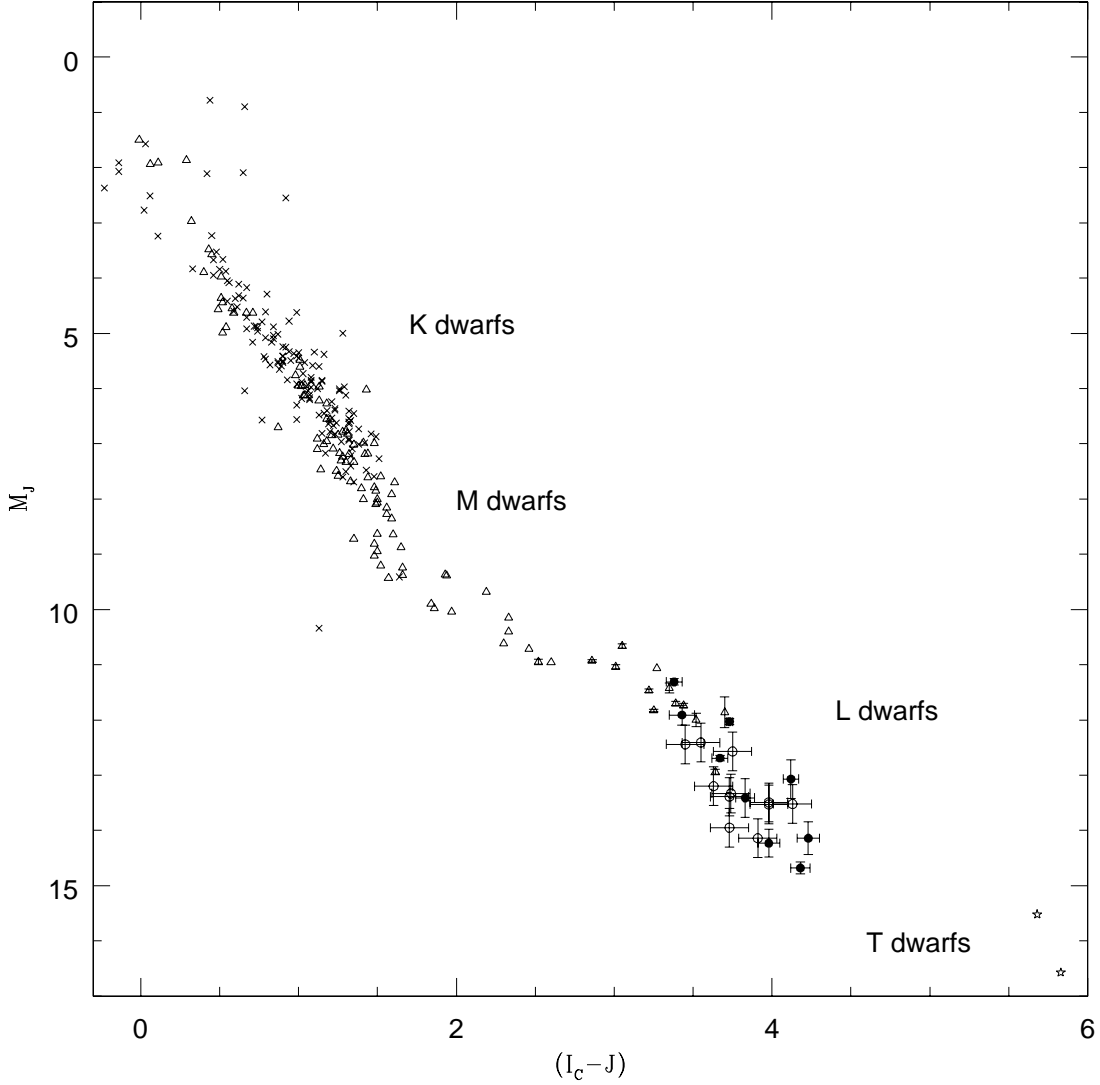


Fig. 2.— The $(M_J, (I_C - J))$ diagram for low-mass dwarfs. Crosses are nearby stars with BVRI data from Bessell (1989), JHK observations from 2MASS and parallax measurements from Hipparcos; open triangles mark nearby, single stars with accurate trigonometric parallax measurements (from Reid & Gizis, 1997b), and late-M/L dwarfs from the USNO parallax program (Dahn *et al.*, in prep); solid points identify the nine L dwarfs in the present HST sample which have trigonometric parallax measurements (Dahn *et al.*); the remaining 11 HST L dwarfs, with spectroscopic parallax estimates, are plotted as open circles; finally, five-pointed stars mark data for the T dwarfs Gl 229B (Nakajima *et al.*, 1995) and Gl 570D (Burgasser *et al.*, 2000).

Fig. 3.— A: HST Planetary Camera images of 2M0746. The left panel shows the F606W exposure; the right panel the F814W image. The field of view is 6×6 arcseconds. (Figures enclosed separately.)

Fig. 3.— B: HST Planetary Camera images of 2M0850. The left panel shows the F606W exposure; the right panel the F814W exposure. The bright object in the upper left corner is an unrelated M dwarf.

Fig. 3.— C: HST Planetary Camera images of 2M0920. The left panel shows the F606W exposure; the right panel the F814W exposure.

Fig. 3.— D: HST Planetary Camera images of 2M1146. The left panel shows the F606W exposure; the right panel the F814W exposure.

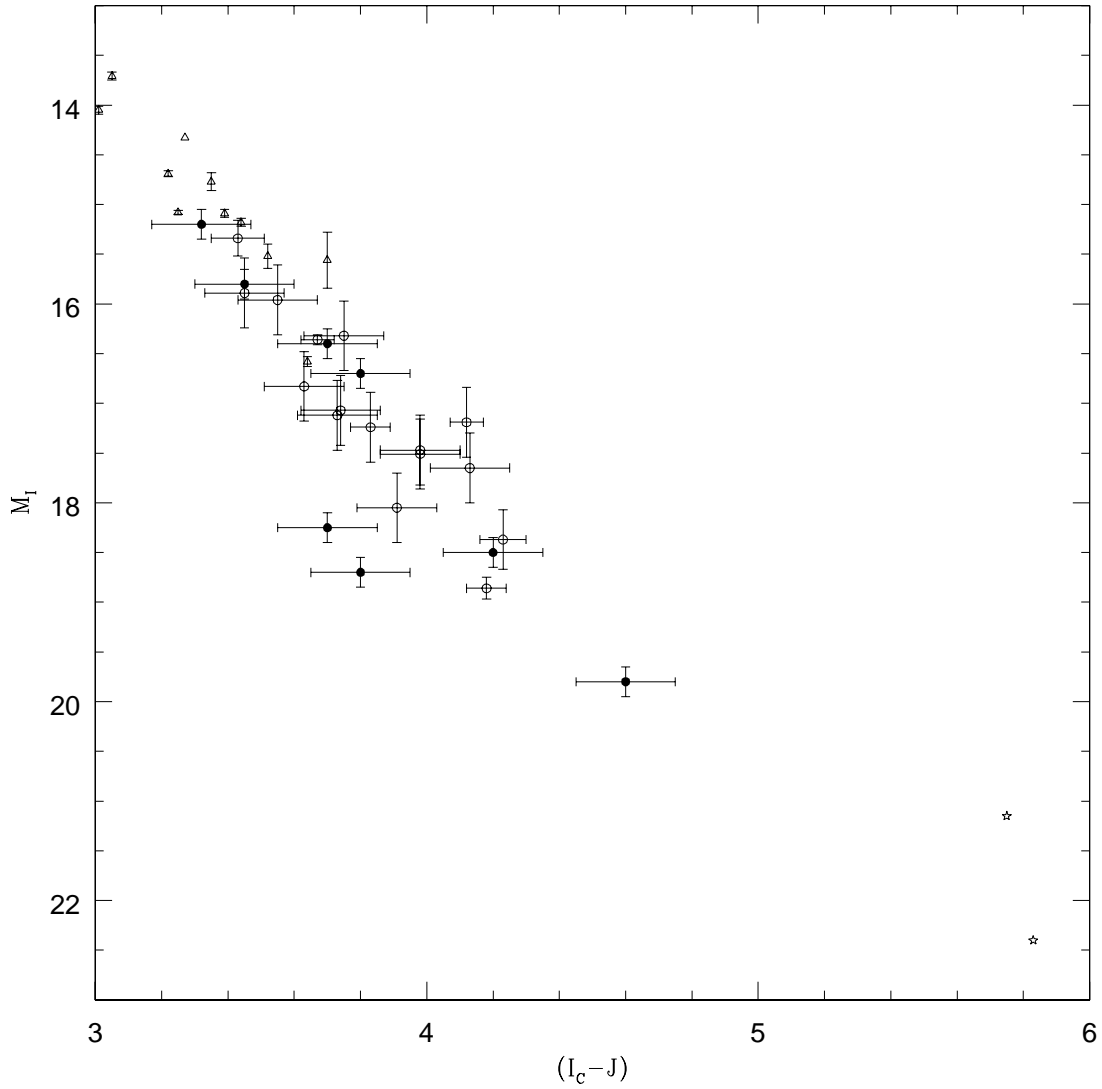


Fig. 4.— The $(M_I, (I_C-J))$ colour-magnitude diagram for ultracool dwarfs. As in figure 2, open triangles mark data for nearby late-type M dwarfs and L dwarfs with trigonometric parallax measurements. The open circles plot data for the apparently single L dwarfs with HST observations; solid points (with errorbars) mark our estimates of the location of the four binary components.

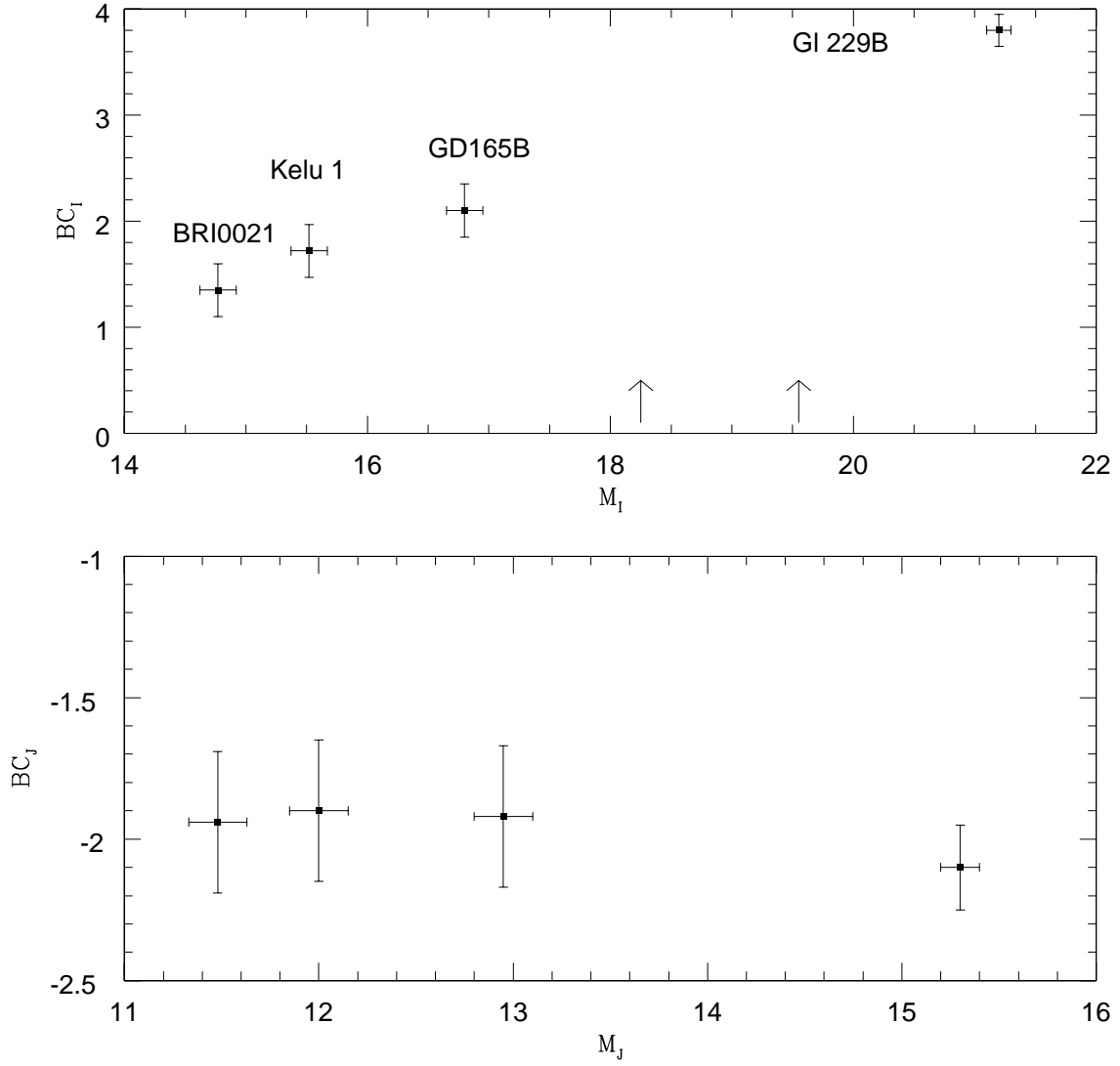


Fig. 5.— Bolometric corrections for late-type dwarfs. The upper panel plots the available data for the Cousins I-band, where the arrows mark the locations of 2M0850A and 2M0850B; the lower panel plots (M_J, BC_J) data for the same four calibrators.

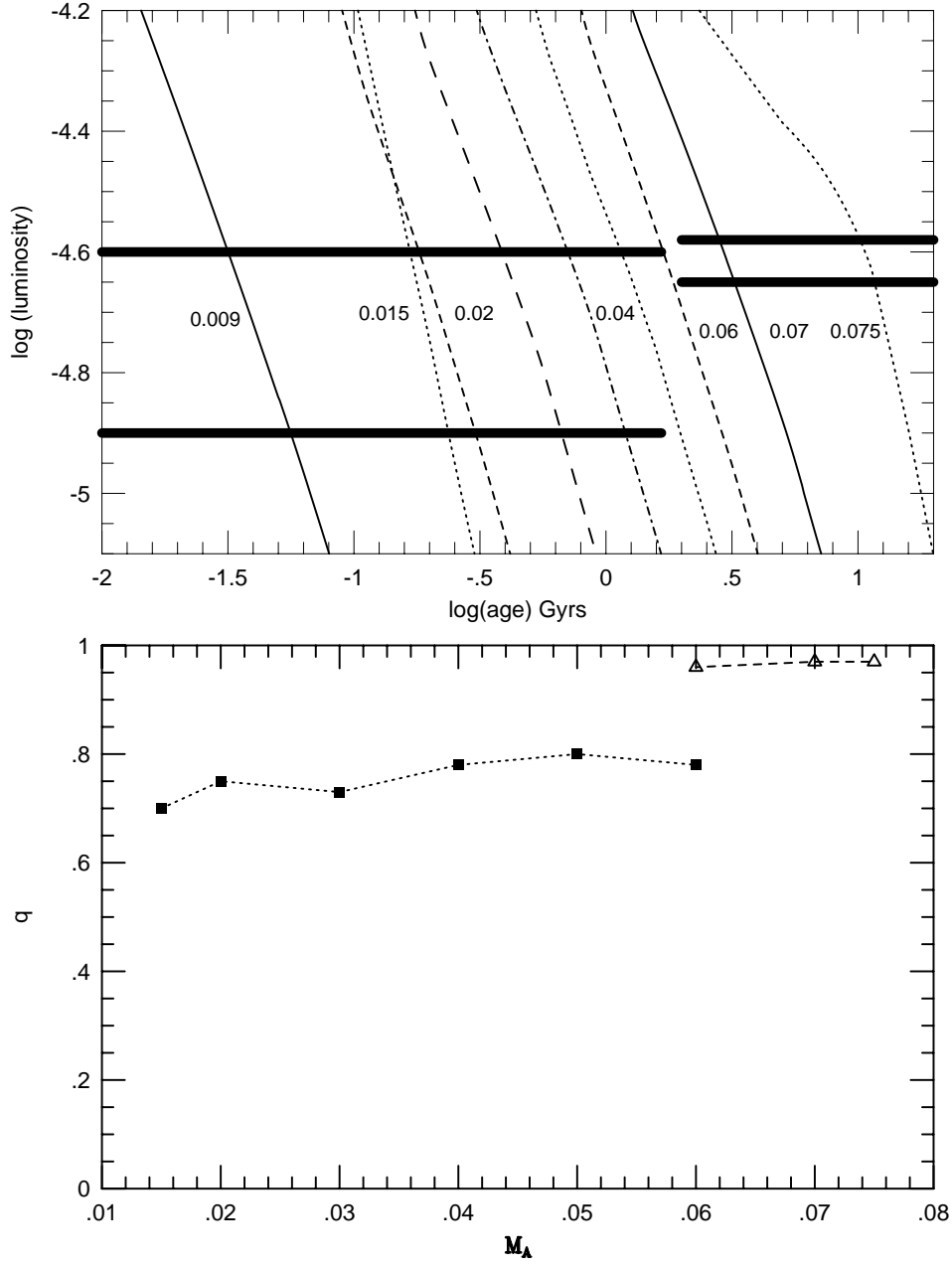


Fig. 6.— Mass estimates for 2M0850AB and 2M0920AB. The upper panel plots evolutionary tracks for brown dwarfs calculated by Burrows *et al.* (1993, 1997). The solid horizontal lines plot the luminosity estimates for the four components: the left pair of lines plot 2M0850A and B, with the upper mass limit for 2M0850A set at $0.06M_{\odot}$ through the detection of lithium; the right-hand pair of lines, closer spaced in luminosity, mark 2M0920A and B. In the latter case, the non-detection of lithium sets a lower mass limit of $0.06M_{\odot}$ for 2M0920B.

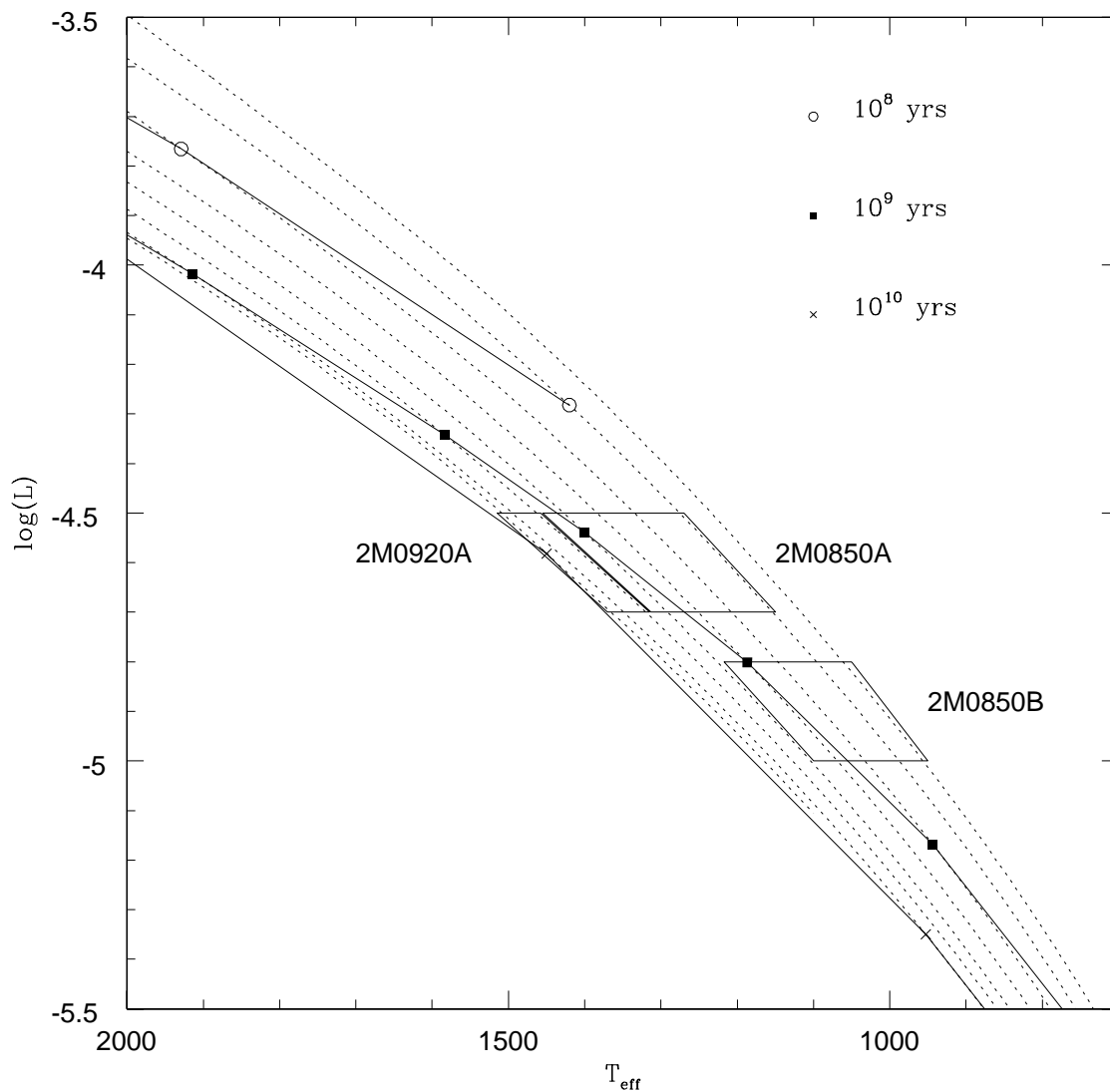


Fig. 7.— Error boxes for the brown dwarf components of 2M0850AB and for 2M0920A (2M0920B is not plotted) superimposed on evolutionary tracks for brown dwarfs from Burrows *et al.* (1997). The solid lines mark 10^8 , 10^9 and 10^{10} year isochrones; the dotted lines mark the evolution of 0.015, 0.02, 0.03, 0.04, 0.05, 0.06, 0.07 and 0.075 M_{\odot} models: the 0.015 M_{\odot} model has the highest luminosity at a given temperature.

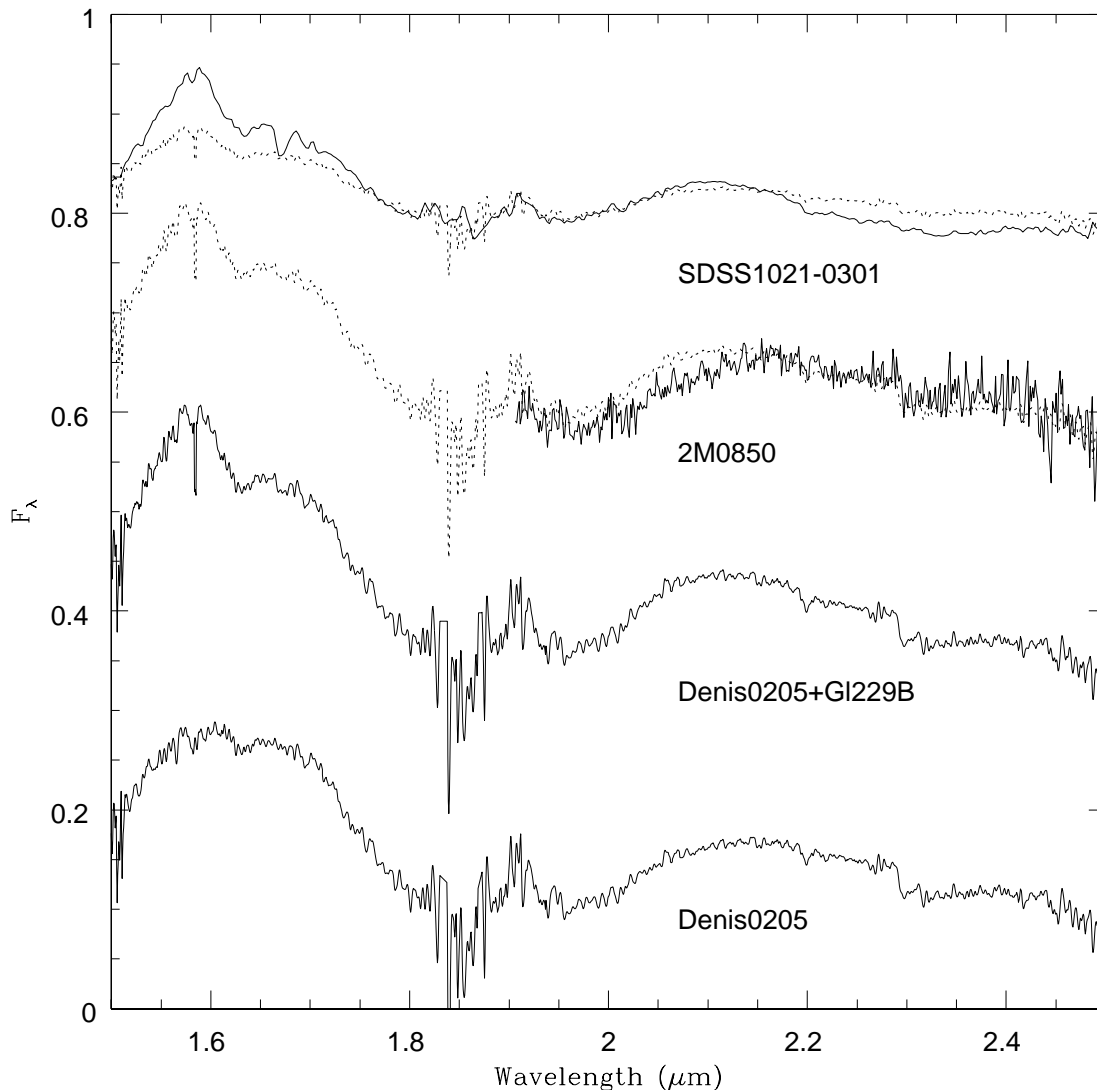


Fig. 8.— The composite 1.5 to 2.5 μm spectrum of a hypothetical late-L/T-dwarf binary. The lowest spectrum plots our CGS4 data for the L7 dwarf, DENIS-P 0205.4-1159; next, we plot the hypothetical binary, combining the DENIS0205 spectrum with data for GI 229B (Geballe *et al.*, 1996), with $\Delta J_{B-A} = 1$ magnitude; third from the bottom, we plot K-band data for 2M0850; the top spectrum plots CGS4 data for the early T-dwarf, SDSS1021-0301 (data courtesy of S. Leggett). The dotted line superimposed on the latter two spectra plots the L/T composite, scaled to match at 2.15 μm .

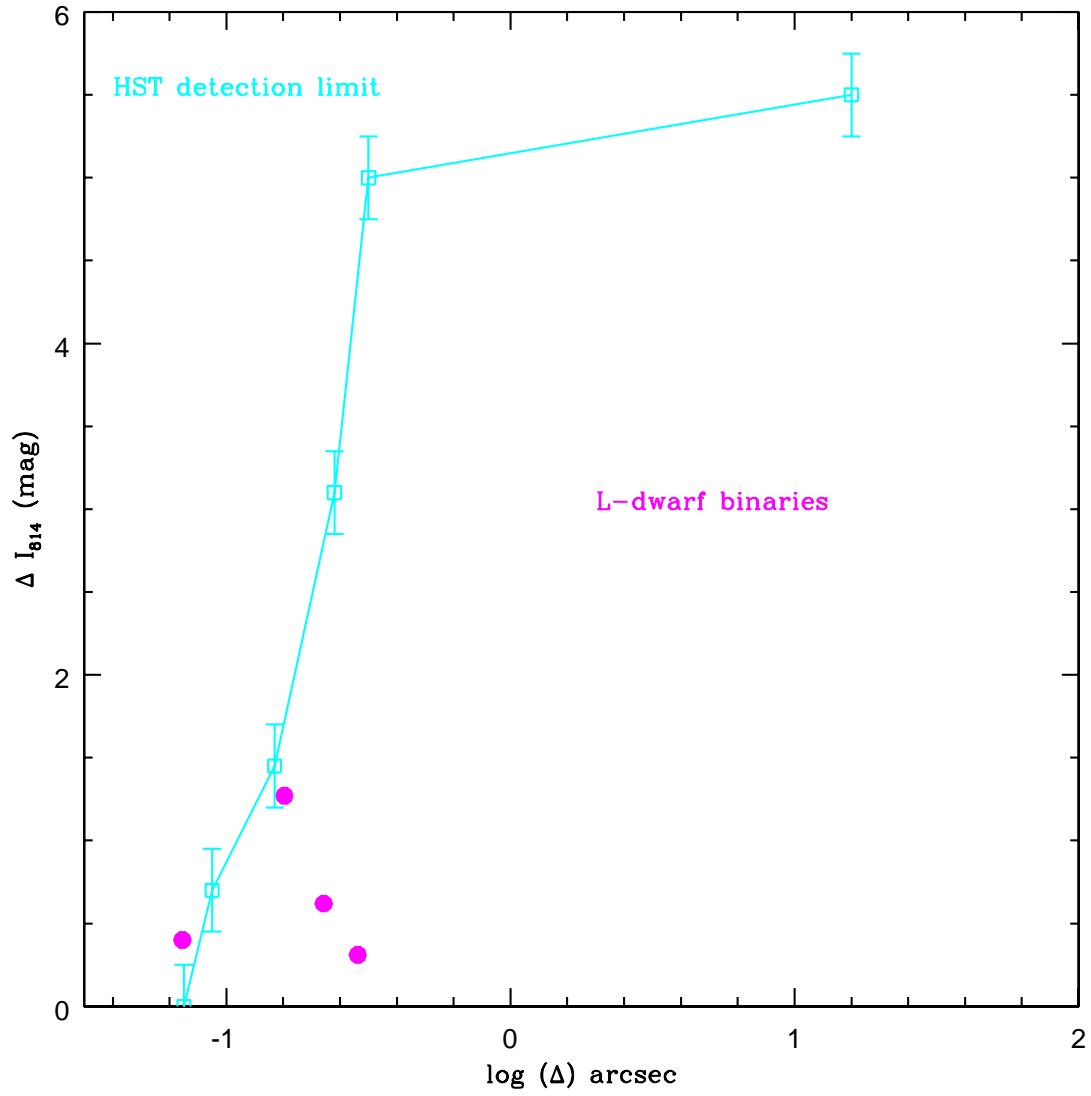


Fig. 9.— A comparison between the observed primary-secondary magnitude difference, δI_{F814} , and the formal detection limits of the HST Planetary Camera observations.

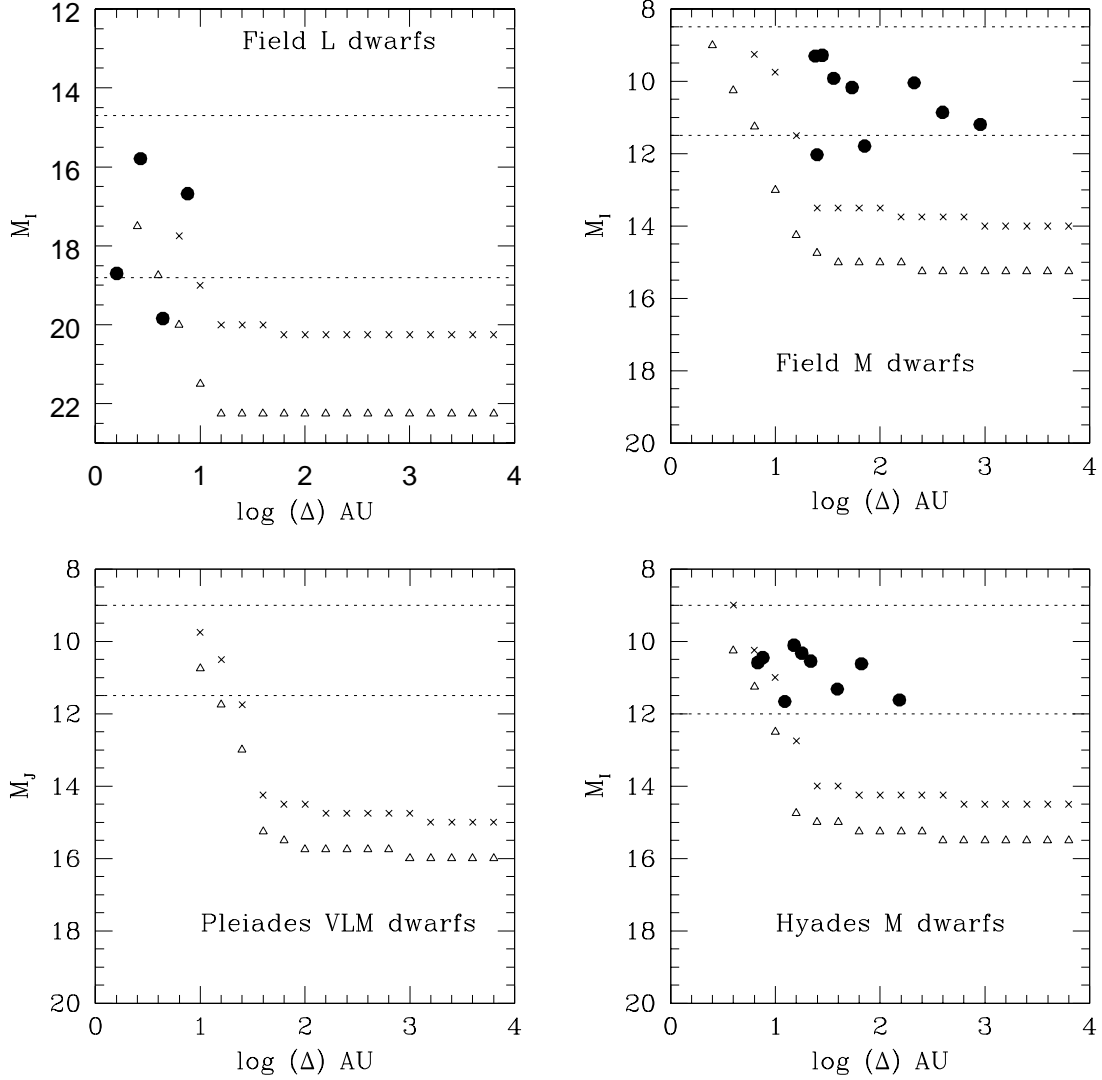


Fig. 10.— Sensitivity limits of four high-resolution imaging surveys for companions. The L dwarf data are from the present paper; field M dwarfs from Reid & Gizis (1997a); Hyades M dwarfs from Reid & Gizis (1997b); and Pleiades data from Martín *et al.* (2000). Note that we plot M_J for the last mentioned dataset. Limiting magnitude (M_I or M_J) is plotted as a function of linear separation from the primary (in AU): crosses mark the 100% completeness level; open triangles, 50% completeness. The horizontal dotted lines indicate the approximate range of absolute magnitudes of the primaries, and detected companions are plotted as solid points.

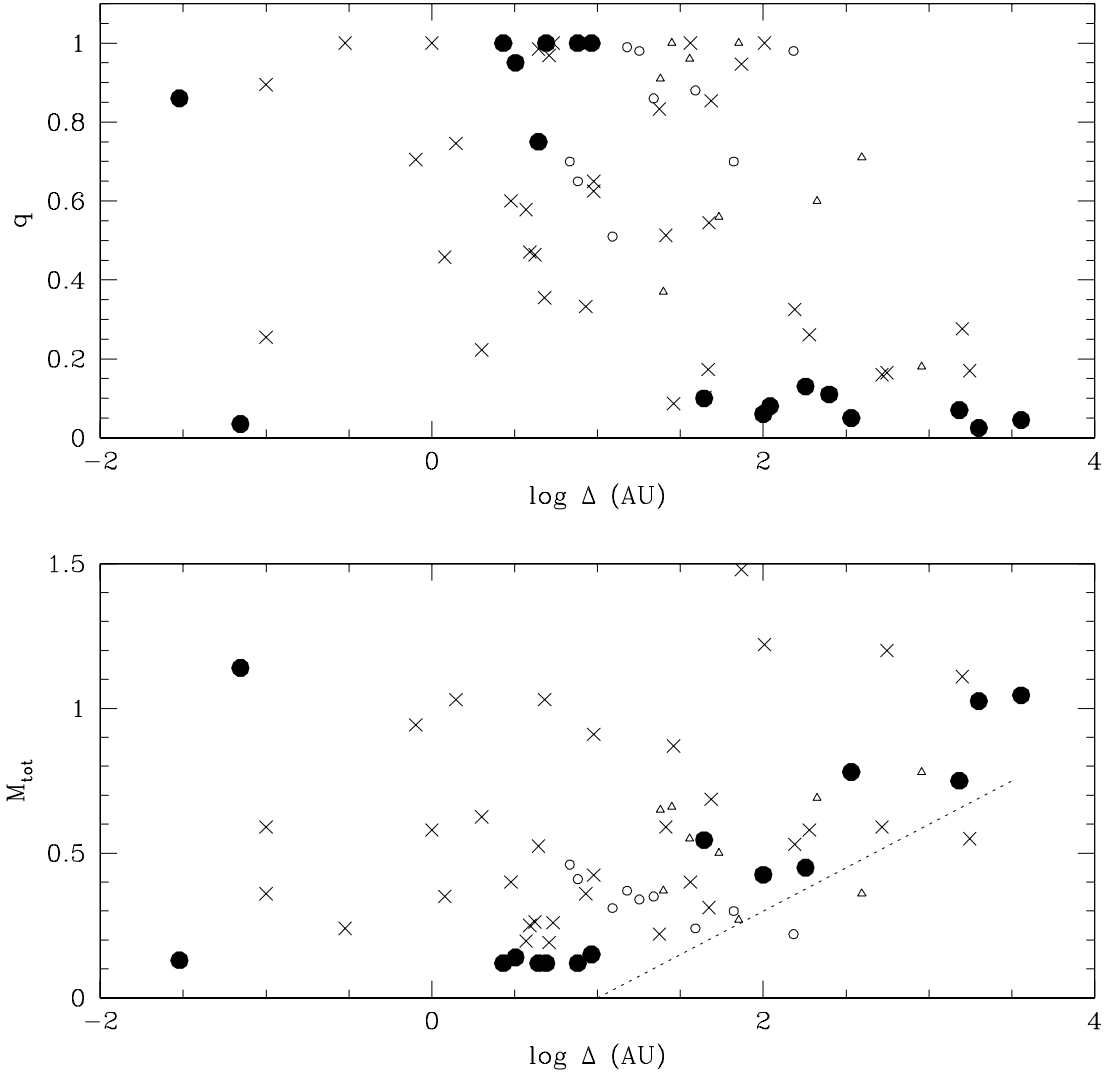


Fig. 11.— The upper panel plots the (mass ratio, $\log(\text{separation})$) distribution for L dwarf binaries from Table 5 (solid point) matched against similar data for M dwarf binaries in the Solar Neighbourhood (crosses) and from the HST Hyades (open circles) and field (open triangles) surveys. The lower panel plots the total mass of each binary against $\log(\Delta)$, using the same symbols.

This figure "0746i.gif" is available in "gif" format from:

<http://arxiv.org/ps/astro-ph/0010202v1>

This figure "0746v.gif" is available in "gif" format from:

<http://arxiv.org/ps/astro-ph/0010202v1>

This figure "2m0850i.gif" is available in "gif" format from:

<http://arxiv.org/ps/astro-ph/0010202v1>

This figure "2m0850v.gif" is available in "gif" format from:

<http://arxiv.org/ps/astro-ph/0010202v1>

This figure "2m0920i.gif" is available in "gif" format from:

<http://arxiv.org/ps/astro-ph/0010202v1>

This figure "2m0920v.gif" is available in "gif" format from:

<http://arxiv.org/ps/astro-ph/0010202v1>

This figure "2m1146i.gif" is available in "gif" format from:

<http://arxiv.org/ps/astro-ph/0010202v1>

This figure "2m1146v.gif" is available in "gif" format from:

<http://arxiv.org/ps/astro-ph/0010202v1>